Report:

Design of an isolated measurement channel for ECG signals

Lucía Chacón Carracedo
Celia Sánchez Laorden

June 9, 2021

UNIVERSITAT DE BARCELONA

Contents

List of Figures

List of Tables

1 Introduction

Throughout this laboratory, an analog channel (front-end) will be developed for the measurement of a biopotential. Specifically, the main objective of this project is to the design a measurement system to perform an Electrocardiography (ECG) of a lead.
The following specific objectives have been identified in order to reach the first aim:

- Study of the heart's electrical activity, its magnitude and frequency.
- To learn the CE classification of electrocardiographs.
- To estimate a cost study for the project of assembling and testing an ECG.
- To analyse all the derivations a electrocardiograph is composed of.
- To study the set-up of an electrocardiograph, its stages and amplifiers, by characterising the structures using LTspice simulation.
- To acquire knowledge of LTspice simulations and experimental generation of circuits on the "Protoboard" to study the filters needed for a clear signal.
- To acquire knowledge of LabView to design a good acquisition user interface.
- To learn how to use the devices required for the simulations and experimental testings: Analog Discovery 2, MyDaq, Oscilloscope, multimeter and function generator.

The executions of this project has been carried out during the second semester under the supervision of Jordi Colomer. The project has entailed a total dedication of 110 hours.

1.1 Context

1.1.1 Electrocardiogram

The ECG technique allows to visualize the electrical activity of the heart over a period of time and thus identify the activity of the myocardium. As is well known, the heart beats

at a certain periodic rate caused by its expansion and contraction facilitating the flow of blood throughout the body. This periodic frequency of activity of the heart is caused by the depolarization of the myocardium, which, in turn, generates the electrical impulses that we can visualize with the ECG.

The electric field that is generated with the depolarization resembles an electric dipole. That is why the electrical activity of the heart is electrically modeled as a movement of electric dipoles. The dipoles are represented by a line that joins the positive and negative charges. This vector is called the Lead.

In this way, since they are differential leads, the resulting electrical signals for each lead are obtained by subtracting the value obtained at the positive point from the other negative point. The resulting derivations are:

- **Lead I**: BI–BD $(LA$–$RA)$
- **Lead II**: PI–BD $(LL$–$RA)$
- **Lead III**: PI–BI $(LL$–$LA)$

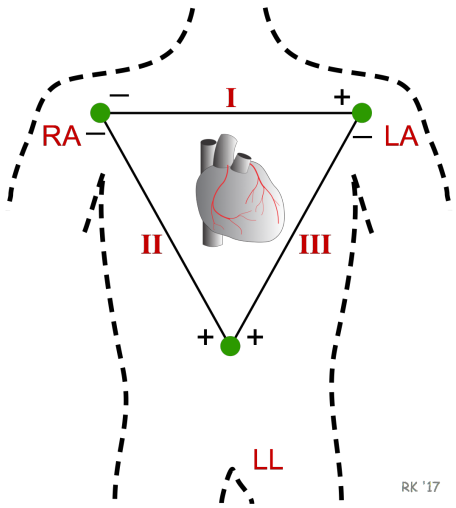

Figure 1.1: Electrical derivations of the heart and their nomenclature

The amplitude of the ECG electrical signal in one of the leads ranges between $0.1mV$ and $3mV$ and a frequency range between $1Hz$ and $50Hz$.

1.1.2 Measurement Channel (Front-end)

The front-end of this project presented the following structure:

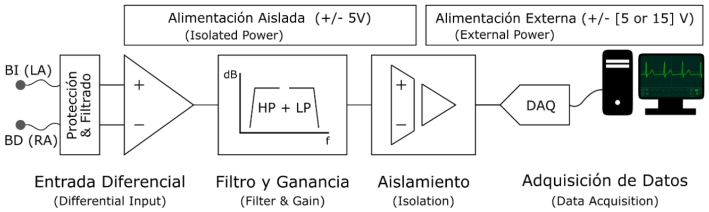

Figure 1.2: Measurement channel for the detection of a biopotential signal of one lead in a electrocardiograph

From left to right it can be seen the connection of the electrodes that were connected to the differential amplifier through a high frequency protection and filtering structure. Next, the amplified differential output was filtered through a post-processing stage made up of high-pass and low-pass filters. Finally, the filtered signal was isolated using an isolation amplifier to be digitized and visualized by a computer.

In order to assembly the measurement channel, this project was divided in four sections:

- 1. Protection Stage and High Frequency Filter
- 2. Differential Amplification
- 3. Post Amplification Stage and Filter
- 4. Isolation, Acquisition and Representation of the Signal

1.1.3 CE classification and Cost Study

Following the application of the Council Directive 93/42/EEC on Medical Devices the electrocardiographs (ECG) are in Class I as their electrodes are non-invasive. In Class I are grouped devices that come into contact only with intact skin or that do not touch the patient.
Finally the cost study of this project is presented in the *Table* 1.3.

Item	Cost
IEC 60601-2-25:2011 - Medical electrical equipment - Part 2-25: Particular requirements for the basic safety and essential performance of electrocardiograph	298,65 €
CSE Database: The Common Standards for Electrocardiography (CSE) Database is a collection of approximately 1000 short (12- or 15-lead) ECG recordings, designed for evaluating diagnostic ECG analyzers. It must be purchased from the INSERM	1.273,85 €
ISO/IEEE 11073-20701:2020 - Health informatics — Device interoperability — Part 20701: Point-of-care medical device communication — Service oriented medical device exchange architecture and protocol binding.	124,84 €
Protoboard	4,95 €
Analog Discovery 2 by Digilent	399 €
NI mydaq by National Instruments	397 €
NI Labview Professional License	5.861,00 €
Set of 480 resistors K/RES-E3 by Velleman Projects	9,90 €
OP467 (2 units)	25,02 €/unit
ISO122JP 98ZDC1H	2,54 €
INA114	10,61 €
LM324N	0,37 €
Capacitors (minimum of two: 47 µF and 122 µF)	0,27 €/ unit (Quantity: 2)
Set of wires	3,23 € / unit (Quantity: 2)
RSDS 1204CFL	1.329,79 €
AFG 21005	332,75 €
RS A3305P	321,86 €
RS14 (multimeter)	36,63 €
Total cost	10.435,75 €

Figure 1.3: Cost Study of the project

1.2 Limitations of the Study and Location

This project was part of the Biomedical Equipment and Instruments subject. The modality of work has been half laboratory work and half teleworking. The last modality represents a first factor of risk for correct execution. For that reason, it has been essential to control and reinforce the communication with the supervisor.

The second restriction has been the time for executing the project. Since part of the time

has been devoted to document (ourselves) as the students (we) do not have previous experience of all the involved tasks.

Moreover, the lack of some types of electrical components have forced to connect resistance in series or in parallel. The lack of space and working with a *protoboard* instead of integrated circuit has produced unwanted noise and has impeded a clean presentation.

Other limitations are the supply range given by the Analog Discovery 2.

2 Detailed Engineering

2.1 Technologies and materials involved

For this project, it was necessary both software and hardware. Two different programs were used: LTSpice and LabView. LTspice is a high performance SPICE simulation software, schematic capture and waveform viewer with enhancements and models for easing the simulation of analog circuits. It is mainly used for general circuit simulation.
Moreover, LabVIEW is a software that provides a powerful graphical development environment for the design of engineering applications for data acquisition, measurement analysis, and data presentation thanks to a programming language without the complexity of other development tools.
For this project LTSpice has been used for all the circuit simulations and LabVIEW for the final testing of the ECG device.
Regarding the hardware, the following *Table* 2.1 summarizes the material used throughout the project:

Item	Quantity
Protoboard	2
IN 114 Op-amp	1
INA114	1
ISO122P	1
Wires	-
Capacitors	-
Resistors	-
Analog Discovery	2
MyDAQ NI	1

Table 2.1: List of material used for this project

The specific values for the capacitors and resistors will be detailed in the upcoming sec-

tions of this project.

2.2 Design

In this section the five stages of the ECG are analysed and documented with the LTSpice simulations.

2.2.1 Protection Stage and High Frequency Filter

The stage of protection with the coupled high frequency filter was the first stage of the ECG. It amplified the signal generated between the two electrodes and removed the high frequency signal. Which was mainly noise signal. For an ECG it is important to reduce as much noise as possible and decrease the movements of the electrodes that could ultimately create artefacts. In addition this first stage ensured a first level of electric protection.
The implemented structure was the one depicted in *Figure* 2.1. This stage was composed only of capacitors and resistors. The protection and high impedance were accomplished through the R_p resistors connected in series with the BD and BI electrodes. These resistors were set to $R_p = 100k\Omega$ and they reduced the current to $1A$.

On the other hand, the filtering was accomplished with the R_p resistors and capacitors C_D and C_S. This type of filter was also known as RFI (Radio Frequency Interference) or Low Pass Filter Network. This filter amplified the AC differential signals $(BI - BD)$ with frequencies between $20kHz$ and $300kHz$. At the same time this filter presented a high impedance at the gate of the filter to ensure the user's protection.

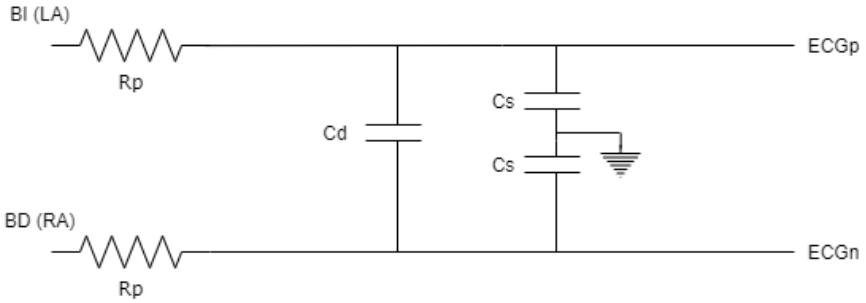

Figure 2.1: Protection and amplification stage at the gate of the ECG. LA and RA nomenclature stands for left and right arm respectively.

From the previous picture the AC output signal $(ECGp - ECGn)$ was the result of the filtered AC input signal $(BI - BD)$. The current analysis is depicted in *Figure* 2.2. The gain of the structure in common mode:

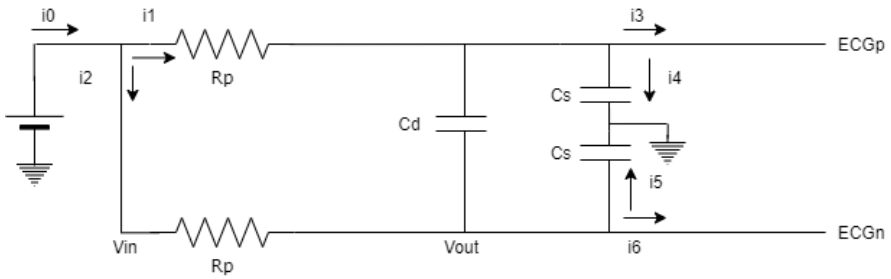

Figure 2.2: Protection and amplification stage at the gate of the ECG. LA and RA nomenclature stands for left and right arm respectively.

$$\frac{V_x - V_{out}}{\frac{1}{C_s S}} + \frac{V_x}{\frac{1}{C_s S}} = -(\frac{V_{out} - V_x}{\frac{1}{C_s S}} + \frac{V_{out}}{\frac{1}{C_s S}})$$

$$V_x = V_{out}$$

$$\frac{V_{in} - V_{out}}{R_p} = \frac{V_{out}}{\frac{1}{C_s S}}$$

$$\frac{V_{out}}{V_{in}} = \frac{1}{1 + R_p C_s S}$$

$$f_D = \frac{1}{2\pi R_p C_s}$$

The gain of the structure in differential mode:

$$f_D = \frac{1}{2\pi R_p (2C_D + C_S)}$$

Regarding the LTSpice simulations, for this first stage two different configurations of the RFI were simulated, one in common mode and a second one in differential mode:

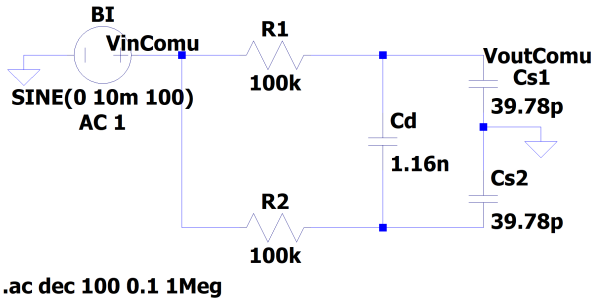

Figure 2.3: RFI in common mode configuration.

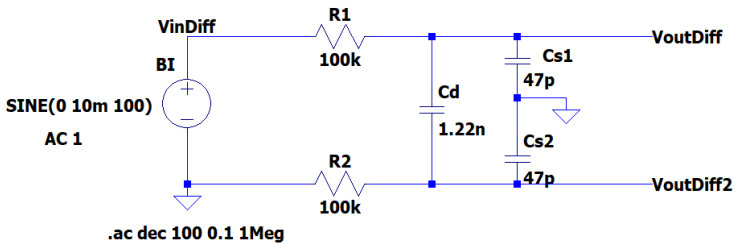

Figure 2.4: RFI in differential mode configuration.

The cut-off frequencies were computed using the BODE simulation for both configurations. Previously the values for the capacitors were selected to have a filter with cut-off frequencies of $f_D = 700Hz(C_D = 1,22nF, C_S = 47pF)$ and $f_C = 40kHz(C_D = 1,16nF, C_S = 39,79pF)$ for the differential and common mode configurations respectively:

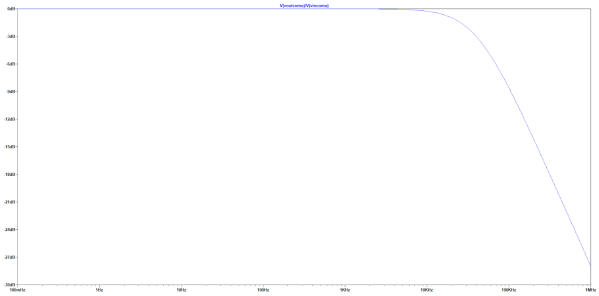

Figure 2.5: BODE of the RFI in common mode configuration.

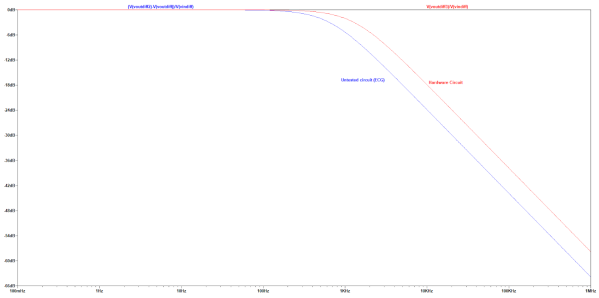

Figure 2.6: BODE of the RFI in differential mode configuration.

The cut-off frequencies computed out of the simulations were:

Frequency	Value (Hz)
f_C	39.95k
f_D	638.54
f_D	1.28k

Table 2.2: Cut-off frequencies of the LFI filter in common and differential modes.

2.2.2 Differential Amplification

In this second stage an Instrumentation Amplifier was needed to amplify the differential signal between both electrodes. This type of amplifiers do only work when both signals have the same Common Voltage value at the gate. In this way, whenever a difference in voltage appears between the two electrodes, the difference is amplified following the gain of the structure. It is very typical to find Instrumentation amplifiers with three Operational Amplifiers ($OPAs$):

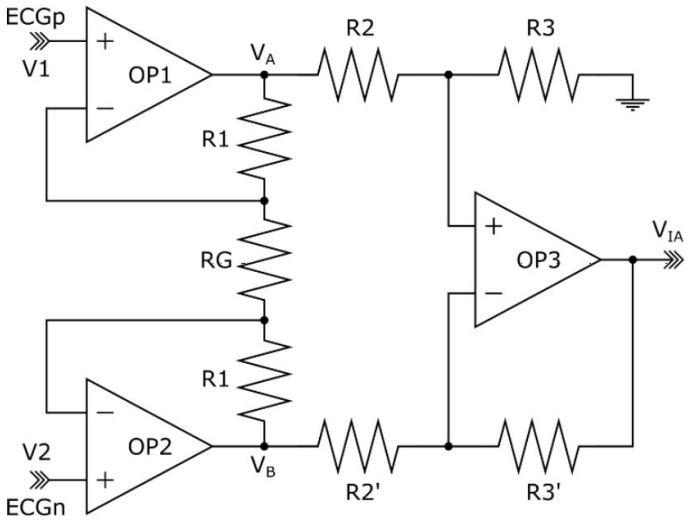

Figure 2.7: Electric schematic of an IA composed of three OPAs, OP_1, OP_2, OP_3

This type of architectures present two gain phases. The first one is composed of the OPAS OP_1 and OP_2, and the resistors R_1 and R_G. The input of this stage is the differential signal $\frac{ECG_p}{V_1} - \frac{ECG_n}{V_2}$ and the output signal is $V_A - V_B$. The second phase consists in the OPA OP_3

and resistors R_2, R'_2, R_3, R'_3, and it has an input signal of $V_A - V_B$ and a final output signal V_{IA}. Finally, the gain of the architecture is calculated as:

$$Gain \quad of \quad the \quad first \quad phase:$$
$$V_A - V_B = i(2R_1 + R_G)$$
$$i = \frac{V_1 - V_2}{R_G}$$
$$Gain \quad of \quad the \quad second \quad phase:$$
$$\frac{V_B - V_{B'}}{R'_2} = \frac{V_{B'} - 0}{R'_3}$$
$$\frac{R'_3}{R'_2} = \frac{V_{B'}}{V_B - V_{B'}}$$
$$Total \quad gain:$$
$$(1) \quad A_{IA} = (1 + \frac{2R_1}{R_G})\frac{R_3}{R_2}(ECG_p - ECG_n)$$

Comparing INA114 versus LM324

During this project two different amplifiers were available to perform this second stage of differential amplification. Those were the $INA114$ [5] and $LM324$ [3] [4] amplifiers. In order to choose the optimal amplifier for this project, both strictures were studied to asses which performs the best. Looking for differences, in the following *Table* 2.3, there are presented their data-sheet main characteristics:

	LM324	**INA114**
Maximum and Minimum Voltage Supply	From $\pm 1.5V to \pm 16V$	From $\pm 2.25V to \pm 18V$
Bandwidth	1 MHz	1 MHz

Table 2.3: IAs datasheet characteristics

From the datasheet two parameters were compared between both amplifiers. The first one was the Maximum and Minimum Voltage Supply. Even though both presented different voltage ranges, the two of them were accepted as possible structures since the voltage supply for this project was set at $\pm 5V$. In addition both had the same bandwidth.

Because both had similar characteristics in terms of voltage and gain range, the analysis has been done through the comparison of their amplifying and common rejection ratio performances. In total two cases were analysed, for a gain of $G_1 = 100\frac{V}{V}$ and $G_2 = 750\frac{V}{V}$ their common and differential mode gains.

LM324 Simulation Performance

Taking into consideration the mathematical gain expression (1) for this structure, the resistances' values were computed for the two cases and established as:

G $\frac{V}{V}$	$R_G\Omega$	$R_1\Omega$	$R_2 = R_2'\Omega$	$R_3 = R_3'\Omega$
100	2k	100k	100k	100k
750	267.02	100k	100k	100k

Table 2.4: Resistances' values for the different gain amplifications.

The LTSpice schematic was the following:

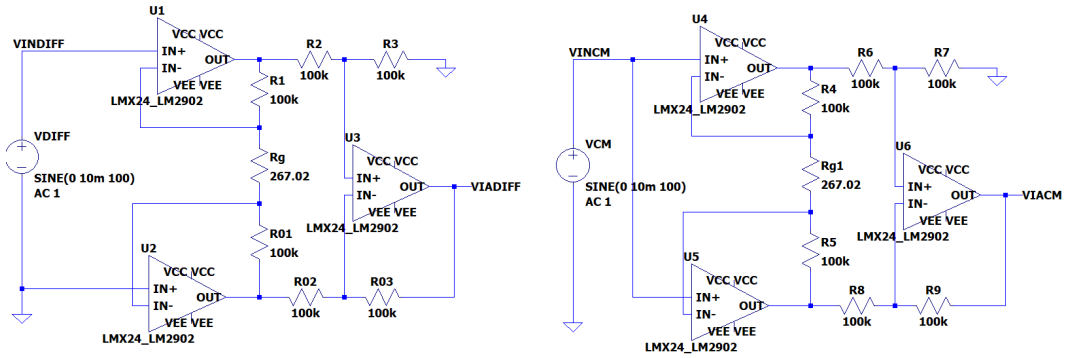

Figure 2.8: On the left the Differential-mode circuit for LM324 at G = 100 $\frac{V}{V}$, on the right the Common-mode circuit for LM324 at G = 100 $\frac{V}{V}$

The BODE diagrams at G = 100 $\frac{V}{V}$:

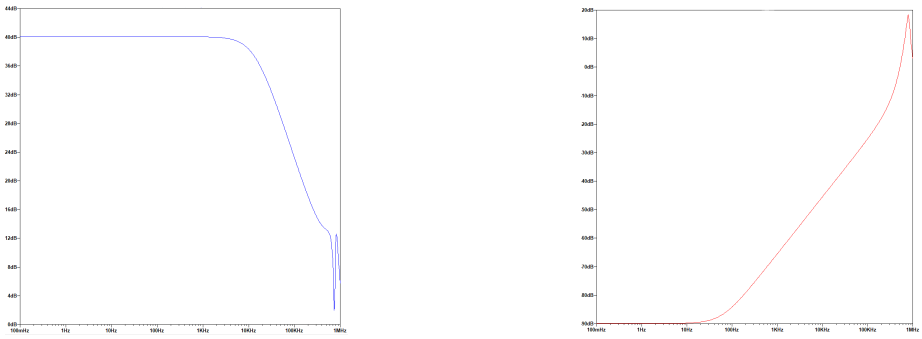

(a) Differential mode configuration

(b) Common Mode configuration

Figure 2.9: BODE of the LM324 at G = $100\ \frac{V}{V}$

The BODE diagrams at G = 750 $\frac{V}{V}$:

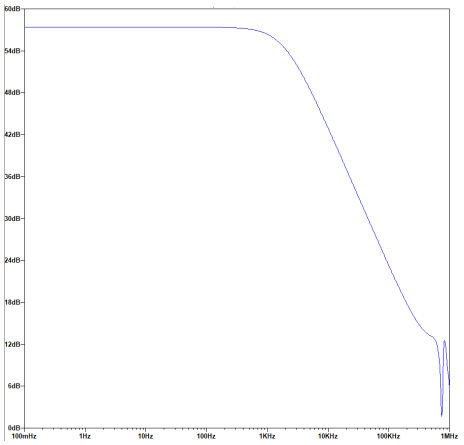

(a) Differential Mode Configuration

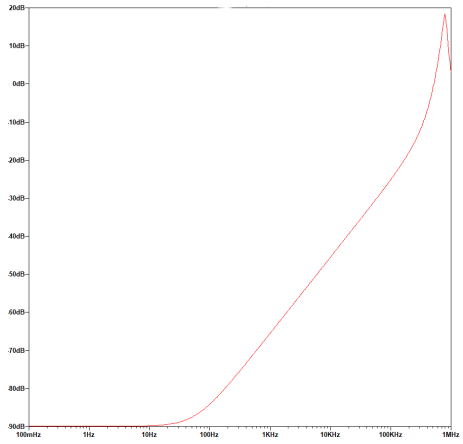

(b) Common Mode Configuration

Figure 2.10: BODE of the LM324 at G = $750\ \frac{V}{V}$

The cut-off frequencies were $f_c = 14, 20kHz$ and $f_c = 1.98kHz$ for the Differential Mode configurations at G = 100 $\frac{V}{V}$ and G = 750 $\frac{V}{V}$ respectively. Next, the CMRR of the LM324 at different gains was simulated. The results were:

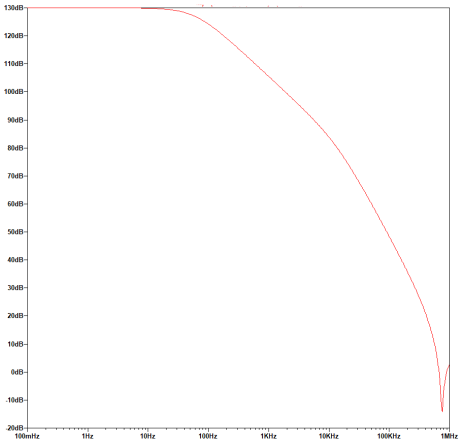

(a) G = 100 $\frac{V}{V}$

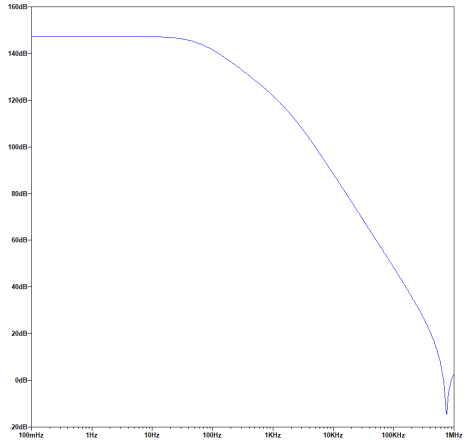

(b) G = 750 $\frac{V}{V}$

Figure 2.11: CMRR simulations for the LM324

Finally a transient simulation was performed to see the overall behaviour of the LM324 at G = 750 $\frac{V}{V}$. The transient simulation was computed with a sinusoidal input signal at the

gate of the structure of 10mV at 10HZ. From the resulted simulation it could be seen easily how the signal was amplified at the output terminal of the structure:

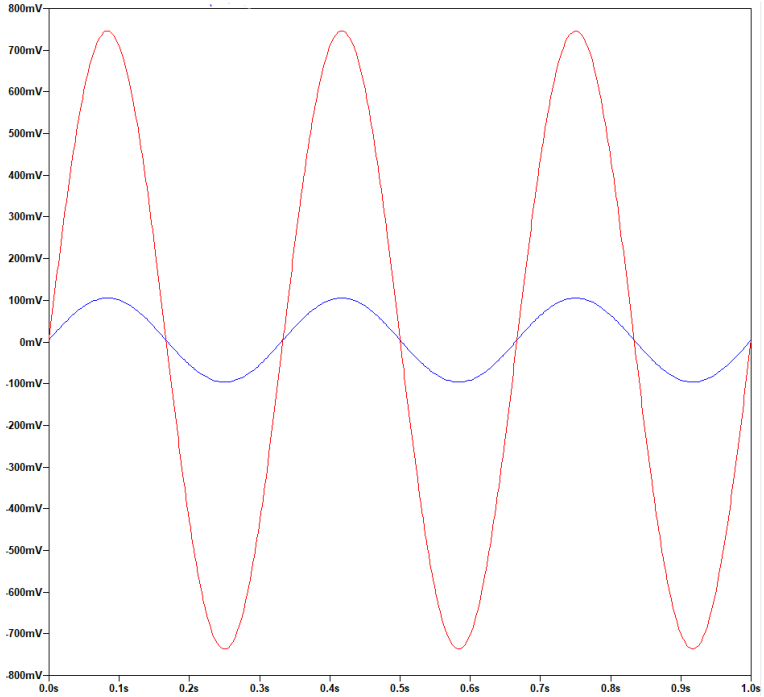

Figure 2.12: Transient simulation for the LM324 with an sinusoidal input signal of 10mV at 10Hz. The red line represents the amplified output signal while the blue one represents the sinusoidal input signal,

After this short characterisation, the LM324 presented the following characteristics:

G $\frac{V}{V}$	$f_c(kHz)$	$CMMR(dB)$**)**
100	14.20	130
750	1,928	144

Table 2.5: Characteriastion of the LM324 structure

INA114 Simulation Performance

The INA114 structure only required of a main resistor, R_G, to fix its gain. This amplifier, used for this project presented all the electronics already embedded inside its structure. So there was no need to add extra resistors, the ones in LM324 known as R_2, R_2', R_3 and

R_3' to fix the gain of the structure. Indeed, the gain of the INA114 was expressed on its data-sheet as:

$$(2) \quad G = 1 + \frac{50k\Omega}{R_G}$$

Considering all resistors in LM324, R_2, R_2', R_3 and R_3', to be equal, the expression in (1) would result in:

$$G_{LM324} = 1 + \frac{2R_1}{R_G}$$

Which resembles the expression (2). Overall, it could be said without demonstration that both might performed similarly. In terms of amplification and Common mode rejection. However the same simulations as with the LM324 were computed to asses the INA114's characteristics. In this way, the following R_G values were established:

G $\frac{V}{V}$	$R_G(k\Omega)$
100	505,05
750	66,76

Table 2.6: R_G values for each Gain

For the simulations with the INA114 amplifier, the schematics of the INA114 symbol from the *Texas Instruments* website have been downloaded and imported into a self-made symbol in LTSpice. The symbol could be seen in *Figure* 2.13 with the entire schematic where it only has been represented the configuration for the G = 100 $\frac{V}{V}$. The case of G = 750 $\frac{V}{V}$ would be the same but changing the value of the R_G.

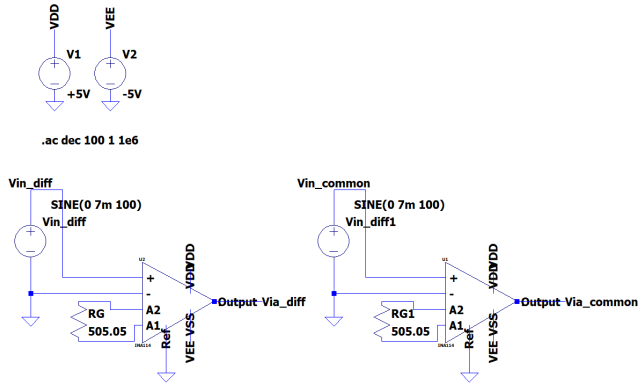

Figure 2.13: On the left the Differential-mode circuit for LM324 at G = 100 $\frac{V}{V}$, on the right the Common-mode circuit for LM324 at G = 100 $\frac{V}{V}$

The BODE diagrams at G = 100 $\frac{V}{V}$:

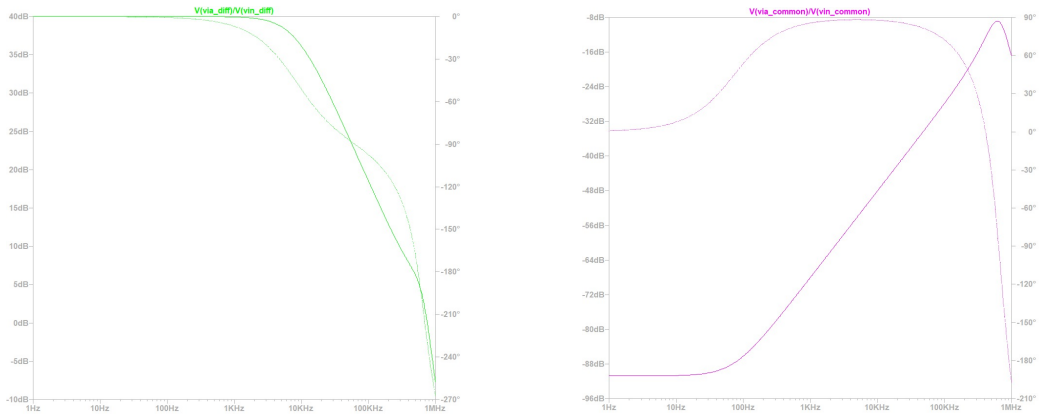

(a) Differential mode configuration (b) Common Mode configuration

Figure 2.14: BODE of the INA114 at G = $100\ \frac{V}{V}$

The BODE diagrams at G = 750 $\frac{V}{V}$:

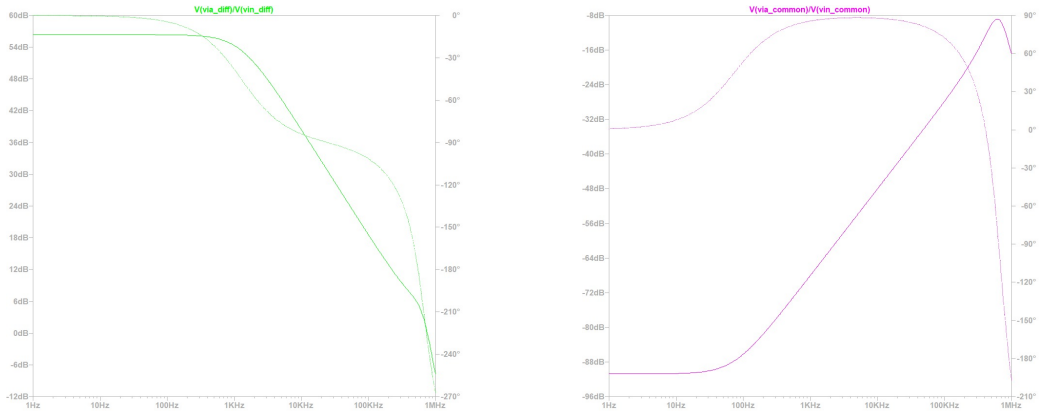

(a) Differential Mode Configuration (b) Common Mode Configuration

Figure 2.15: BODE of the INA114 at G = $750\ \frac{V}{V}$

The cut-off frequencies were $f_c = 8,4kHz$ and $f_c = 2,21kHz$ for the Differential Mode configurations at G = 100 $\frac{V}{V}$ and G = 750 $\frac{V}{V}$ respectively. Next, the CMRR of the INA114 at different gains was simulated. The results were:

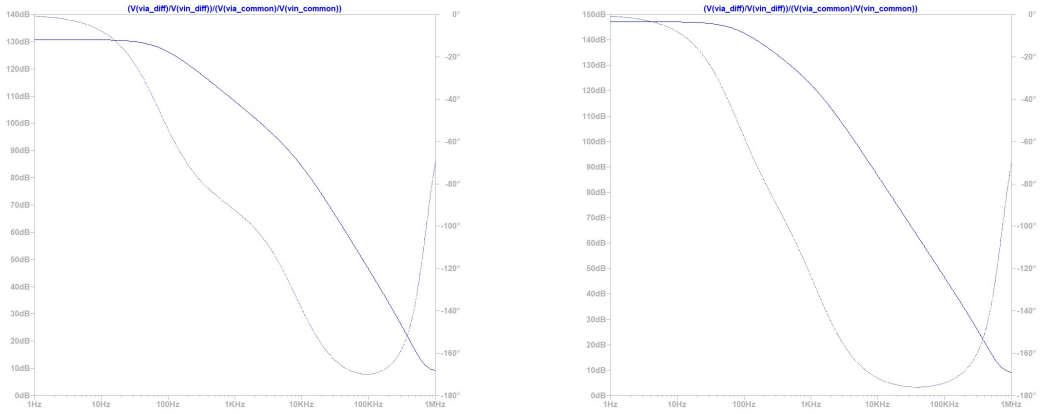

(a) G = 100 $\frac{V}{V}$ (b) G = 750 $\frac{V}{V}$

Figure 2.16: CMRR simulations for the LM324

Finally a transient simulation was performed to see the overall behaviour of the INA114 at G = 750 $\frac{V}{V}$. The transient simulation was computed with a sinusoidal input signal at the gate of the structure of 7mV at 100HZ. From the resulted simulation it could be seen easily how the signal was amplified at the output terminal of the structure:
After this short characterisation, the LM324 presented the following characteristics:

G $\frac{V}{V}$	$f_c(kHz)$	$CMMR(dB)$
100	8,4	131
750	2,21	144

Table 2.7: Characteriastion of the LM324 structure

Finally, comparing the simulations and their results in *Table* 2.5 and*Table* 2.7, it could be concluded that both amplifiers were similar and performed the same when amplifying and rejecting the common mode signal. Hence, none of them could had been discarded based on the characterisation with the LTSpice simulations. In this way, an ultimate experimental testing has been performed to choose the final Instrumentation amplifier. The experimental approach is explained in the upcoming *Section* 2.3.

2.2.3 Post Amplification Stage and Filter

First order active filter

This third filtering stage was composed of two phases. The first filter module consisted in designing and implementing an active low pass filter. The filter scheme is shown in *Figure* 2.19. This first filter will have the function of eliminating the impact of those electrical

signals with frequencies higher than 1000 Hz. Moreover, because it is an active filter, it will amplify the signals with frequencies below the cutoff frequency with an adjustable gain.

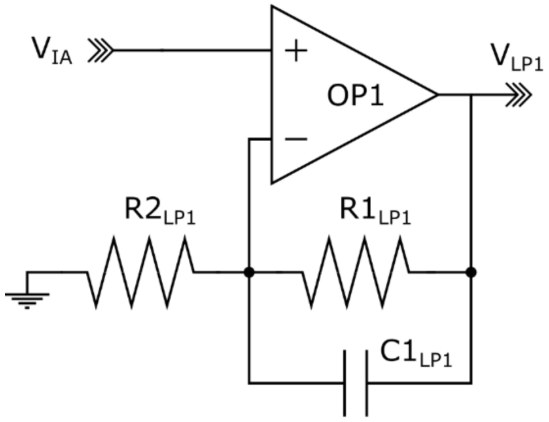

Figure 2.17: First order active filter with adjustable gain.

The gain and cut-off frequencies of the structure were computed and defined as:

$$Z_f = \frac{R_1}{1 + R_1 C S}$$

$$\frac{V_-}{R_2} = \frac{V_{LP1} - V_-}{Z_f}$$

$$V_-(\frac{1}{R_2} + \frac{1}{Z_f}) = \frac{V_{LP1}}{Z_f}$$

$$V_{IA}(1 + \frac{R_1}{R_2 + R_1 R_2 C S}) = V_{LP1}$$

$$(4) \quad \frac{V_{LP1}}{V_{IA}} = 1 + \frac{R_1}{R_2}\frac{1}{1 + R_1 C S}$$

$$(5) \quad f_c = \frac{1}{2\pi R_1 C_1}$$

For a specific gain of $A = 25dB$ the resistors and capacitors values were established as:

$A_{LP1}(dB)$	$A_{LP1}(V/V)$	$f_c(Hz)$	$C_{LP1,1}(F)$	$R_{LP1,1}(\Omega)$	$R_{LP1,2}(\Omega)$
25	17.78	1250	1n	127.32k	7.58k

Table 2.8: Resistors and capacitor values for the specific gai of A = 25dB

For the BODE simulation in LTspice, a symbol was downloaded from the *Texas Instruments* website. The schematic of the simulations and its BODE are depicted in the following figures:

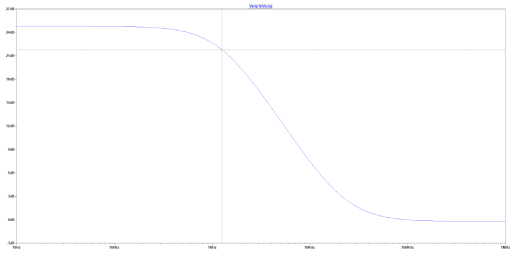

(a) BODE simulation for $A = 25dB$

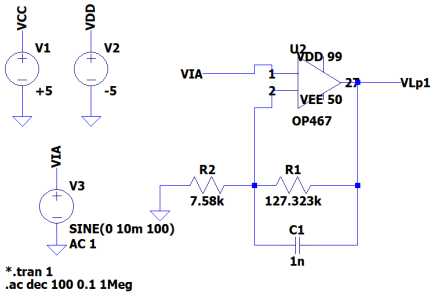

(b) LTspice schematics

Figure 2.18: First order active filter

As it can be seen in *Figure* 2.18a, the @DC gain was accomplished with a final value of $25dB$. The cut-off frequency from the simulation was $1.255KHz$. To check the filter's amplification performance, a transient simulation was also analysed with a sinusoidal input signal of $10mV$ and $100Hz$. Since the input signal's frequency was lower than the cut-off frequency, the output signal was amplified by a factor of 17.78:

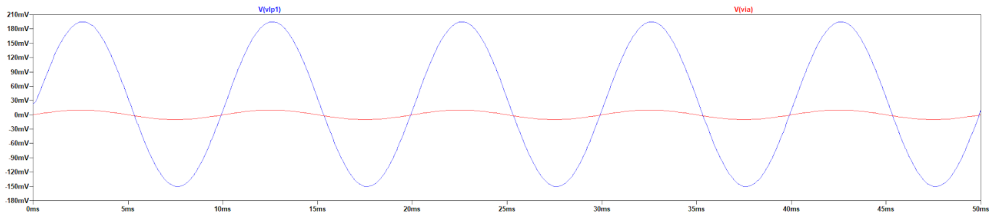

Figure 2.19: Transient simulation with the first order active filter. Sinusoidal input signal of $10mV$ and $100Hz$

Sallen-Key filter

The Sallen-Key structure is an active type of amplifiers based on the use of an non-inverting operational amplifier and two resistors. It can be used to create a circuit VCVS or Voltage-Controlled Voltage-Source, that can also filter (by adding capacitors to the circuit). This second low-pass filter had the responsibility to eliminate the impact of the electrical signals with frequencies above 50 Hz. In addition, as it was a second-order filter, the attenuation

ratio was 40 dB/dec; twice that of a first-order filter. At the same time, because it was an active filter, it amplified the signals with frequencies lower than the cut-off frequency. The following demonstration of the filter has helped to determine its correct behavior:

$$\frac{Vo}{Vi} = \frac{1}{\left(\frac{S}{\omega o}\right)^2 + \frac{1}{Q}\frac{S}{\omega 0} + 1} \rightarrow s = j\omega$$

$$\frac{V_i}{RA_{SK}} = V_\circ \frac{R2_{SK}}{R2_{SK} + R1_{SK}}\left[\frac{1}{RA_{SK}} + \frac{SRB_{SK}CB_{SK}}{RA_{SK}} + \frac{1}{RB_{SK}} + \frac{SRB_{SK}CB_{SK}}{RB_{SK}} - \frac{1}{RB_{SK}} + SCA_{SK} + \right.$$

$$\left. S^2CA_{SK}CB_{SK}RB_{SK} - SCA_{SK}\left(\frac{R2_{SK} + R1_{SK}}{R2_{SK}}\right)\right]$$

$$K = 1 + \frac{R1_{SK}}{R2_{SK}}$$

$$\frac{V_o}{V_i} = K\frac{R2_{SK}}{1 + SRB_{SK}CB_{SK} + SRA_{SK}CB_{SK} + SRA_{SK}CA_{SK} + S^2SRA_{SK}RB_{SK}CB_{SK}CA_{SK} - SRA_{SK}CA_{SK}K}$$

$$\frac{1}{Q\omega o} = (RA_{SK} + RB_{SK})CB_{SK} + (1 - K)RA_{SK}CA_{SK}$$

$$\omega o = \frac{1}{\sqrt{RA_{SK}RB_{SK}CB_{SK}CA_{SK}}} \rightarrow fc = \frac{1}{2\pi\sqrt{RA_{SK}RB_{SK}CB_{SK}CA_{SK}}}$$

$$Q = \frac{\sqrt{RA_{SK}RB_{SK}CB_{SK}CA_{SK}}}{(RA_{SK} + RB_{SK})CB_{SK} + (1 - K)RA_{SK}CA_{SK}}$$

Again, for the specific gain of $3dB$ and cut-off frequency of $f_c = 26Hz$, the following parameters for the resistors and capacitors were established:

$A_{LP1}(dB)$	$f_c(Hz)$	$C_{LP1,1}(F)$	$R_{LP1,1}(\Omega)$	$R_{LP1,2}(\Omega)$
3	1250	1n	127.32k	7.58k

Table 2.9: Resistors and capacitor values for the specific gain of A = 3dB and cut-off frequency of 26Hz

And the final schematic in LTspice and the BODE for the Sallen-Key:

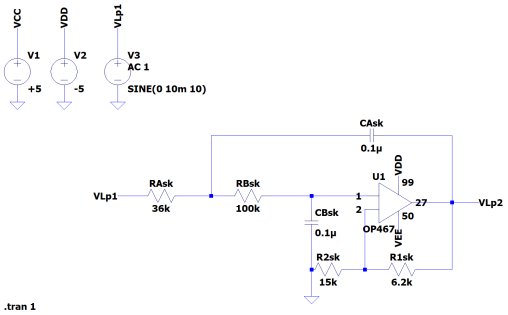

(a) LTSpice schematic

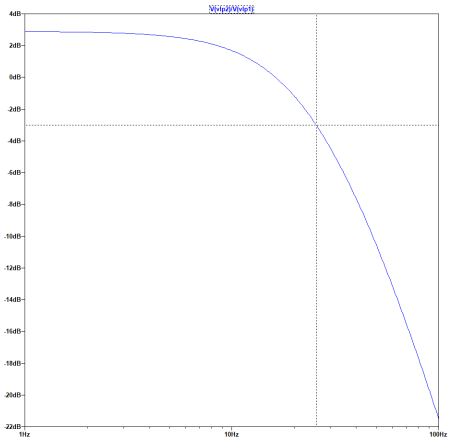

(b) LTspice schematics

Figure 2.20: BODE simulation for $A = 3dB$

The @DC gain and cut-off frequency obtained at the LTSpice simulation in *Figure* 2.20b were $2.867dB$ and $f_c = 25.618Hz(at - 3.010dB)$ respectively. Next a transient simulation was performed with a sinusoidal input signal of $10mV$ and $10Hz$:
As it can be seen in *Figure* 2.21 there was an Offset voltage of $28mV$. This output was not completely random since the data-sheet did specified that this structure presented a Low-Voltage offset at the output gate. This offset might be removed with an high-pass filter.

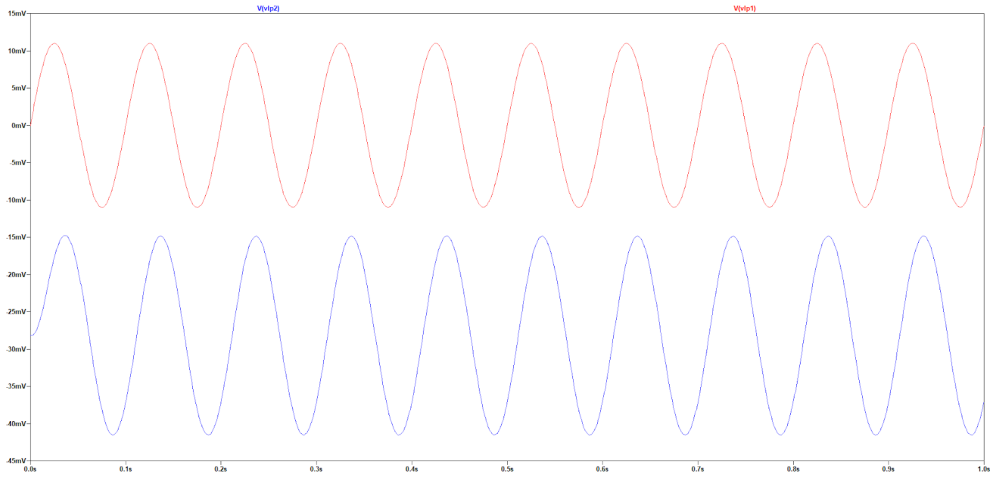

Figure 2.21: Transient simulation for the Sallen-Key. Sinusoidal input signal of $10mV$ and $10Hz$. The red line represents the signal at the input and the blue one at the output.

Cascade Filter

Now both filters are connected so the output signal of the first order active filter is now the input signal of the Sallen-Key. The total gain of the structure in dB is the sum of each filter's gain.

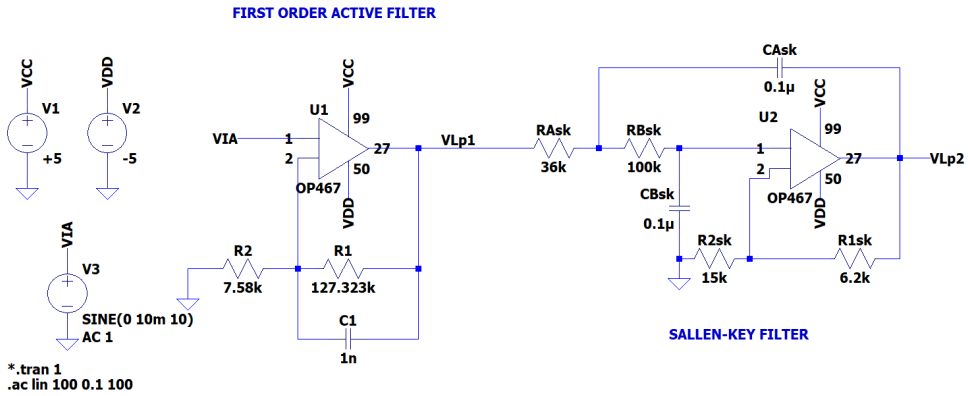

Figure 2.22: LTspice schematic for the final cascade filter.

The cascade filter presented a final gain of $28dB$ and a cut-off frequency of $16.60Hz$:

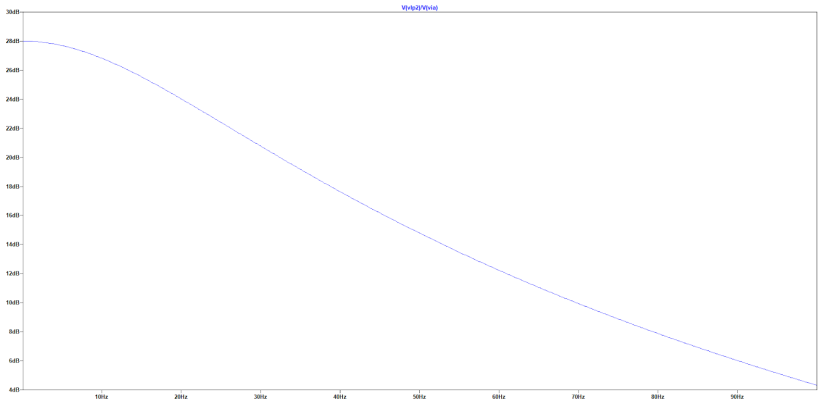

Figure 2.23: Bode for the cascade filter. It can be seen how the final gain is the sum of each gain's filter.

Finally, a transient simulation with a sinusoidal input of $10mV$ and $10Hz$ was performed to analyse the cascade amplifying performance. From the graph below, it could be seen how the input signal at the gate of the first active filter, the red line, was amplified all through the cascade configuration. The ouput signal of the first active filter was represented in green and the final output signal of the cascade configuration in blue. It can be noticed how the larger the amplification, the more phase added to the signal.

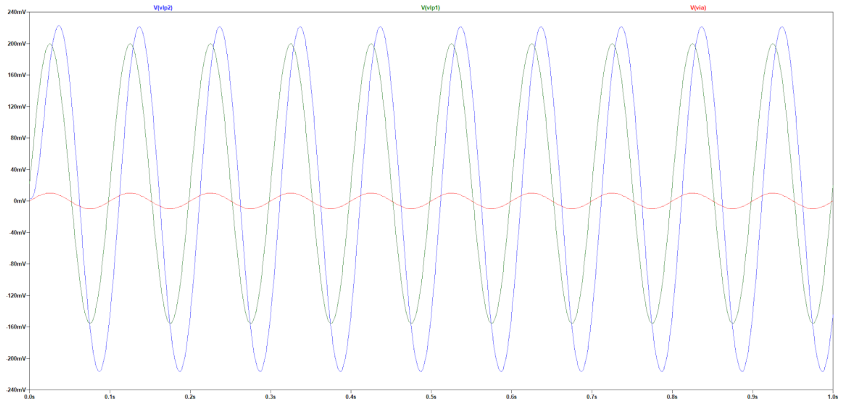

Figure 2.24: Transient simulation for the Sallen-Key. Sinusoidal input signal of $10mV$ and $10Hz$. The red line represents the signal at the input and the blue one at the output..

2.2.4 Isolation, Acquisition and Representation of the Signal

In order to ensure the safety of the patient an isolation stage has been implemented. The Electronic Isolation or EI it is also important to prevent the devices from discharges

originated by the patient, line frequency interference or overvoltage.

Over the different possibilities available in the market, in this project has been used an isolation amplifier, the ISO122 form Texas Instruments [2]. It includes a circuit that provides the analog isolation. The method used by the amplifier to isolate the front panel is a differential capacitive barrier of 2pF (see in Figure 2.25). The input signal is modulated (varying the amplitude) and the modulator acts as a comparator. The resulting signal is triangular with 50% of duty cycle. The demodulator detects the signal transitions through a capacitive barrier and then a switched current source is sent to an integrator (A2). Thanks to a feedback current, the output signal is leveled with the input signal. From this demodulation process, oscillations have been generated that are eliminated with a power supply filtering connected to the output. The ISO122 has a wide range of power supply voltages, in this project it is used ± 5V.

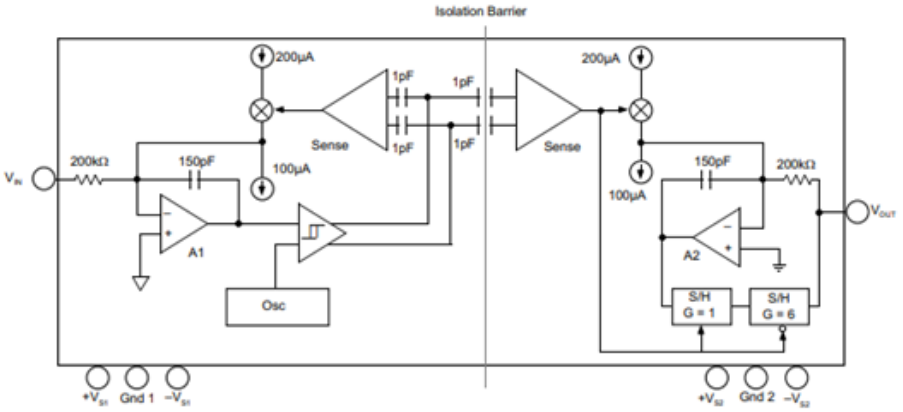

Figure 2.25: Detail of the ISO122 circuit.

The ISO122 has an input voltage range from ± 10 V to ± 100 V and an output voltage range from ± 10 V to ± 12’5 V. Since the low pass filter contains the OP467 amplifier [1] supplied at ± 5V (see in Figure 2.26), the output voltage will be between this range. The maximum gain bandwidth is 50 kHz.

The behaviour of the low pass filter connected to the ISO122 has been checked theoretically with LTSpice (see in Figure 2.27).

The simulated BODE diagram of the low pass filter is presented below.

The cut-off frequency is 63 kHz.

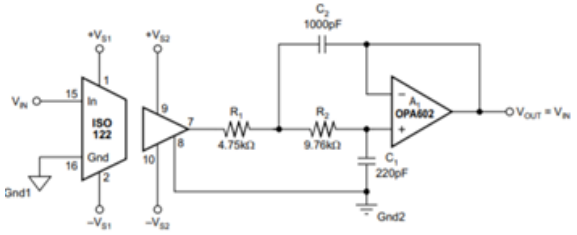

Figure 2.26: Detail of the low pass filter.

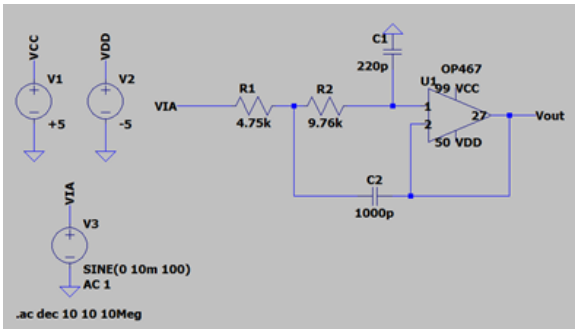

Figure 2.27: Low pass filter LTSpice schematic.

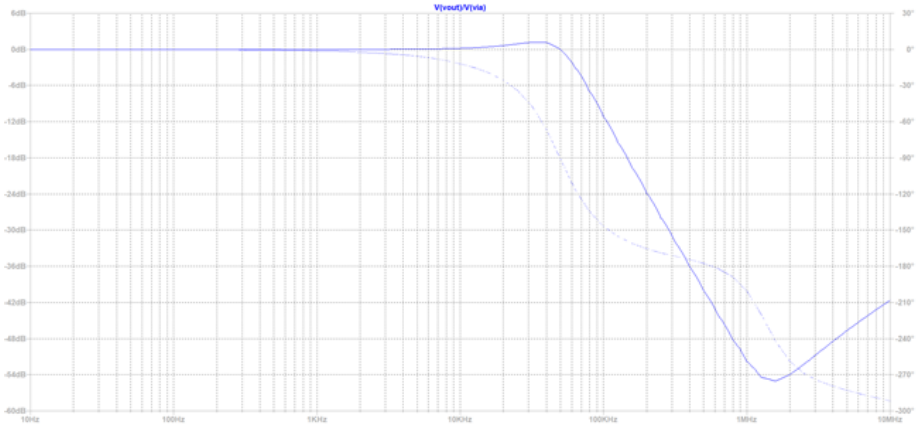

Figure 2.28: Bode diagram simulated by LTSpice.

2.2.5 Verification of the Design

The last section consists on the evaluation of the entire circuit.

The assembly has been done following the schematic seen in Figure 2.29 with the values provided by the Table 2.10. This way, the resistors connected in series have been substituted for resistors that could be found in the lab.

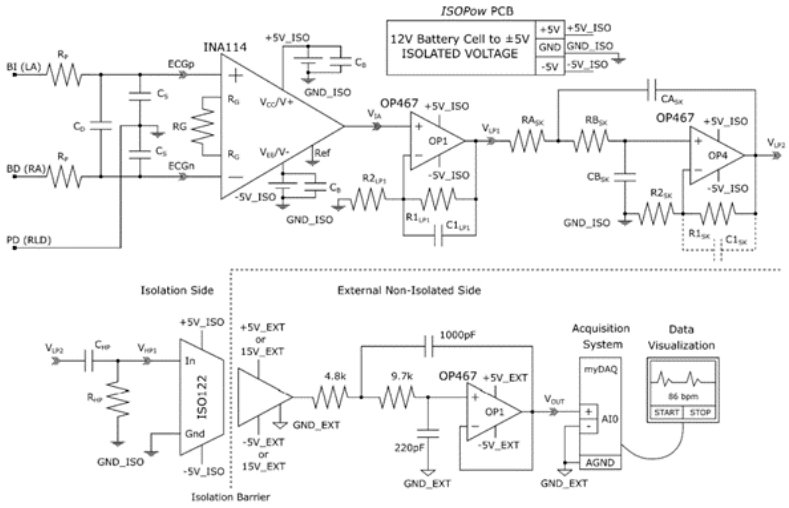

Figure 2.29: Electric scheme of the whole system.

The simulation with LTSpice is presented below. But, previously the theoretical value of R_G has been computed in Table 2.11 for a total gain of 100 V/V and 1000 V/V.

The gains of the amplifiers connected in cascade are multiplied. The stage of the first order active low-pass filter has a gain of 38.03 (V / V) and the stage of the second order Sallen-Key active low-pass filter of 2.79 (V / V). The gain of the isolating amplifier is 1 (V / V).

For the case of a gain of 100 (V / V), it has been chosen a very high INA resistance. This way this stage does not provide a gain.

The LTSpice schematic of the front-end can be visualized in Figure 2.30.

The gain and the cut-off frequency has been simulated for each stage and for the entire schematic in Figure 2.30 using the value for $R_G = 5.9k\Omega$.

For the INA114 stage the cut-off frequency is 673.28 Hz and the gain 9.5 (V/V), see in Figure 2.31a.

Component	Value	Units
CD	1n	F
CS	27p	F
RP	100k	Ω
R1LP1	100k	Ω
R2LP1	2k7	Ω
C1LP1	1n	F
RASK	10k	Ω
RBSK	15k	Ω
CASK	33n	F
CBSK	220n	F
R1SK	100k	Ω
R2SK	56k	Ω
C1SK	10n	F
RHP	1M	Ω
CHP	1u	F

Table 2.10: Passive components used in the final verification.

A_T	R_G	Units
100	1G	Ω
1000	5.9k	Ω

Table 2.11: R_G values.

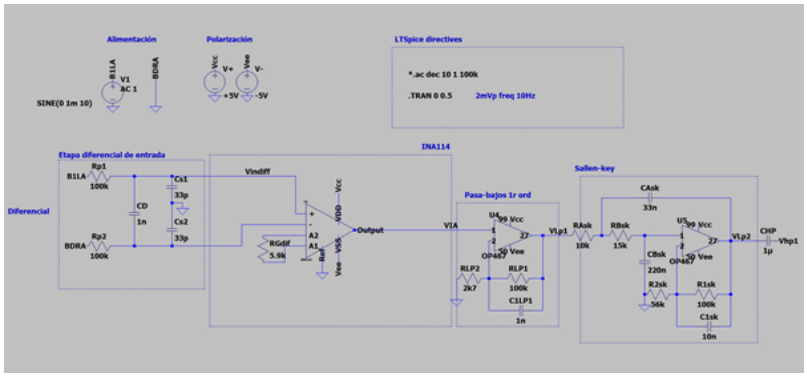

Figure 2.30: LTSpice schematic of the ECG front-end.

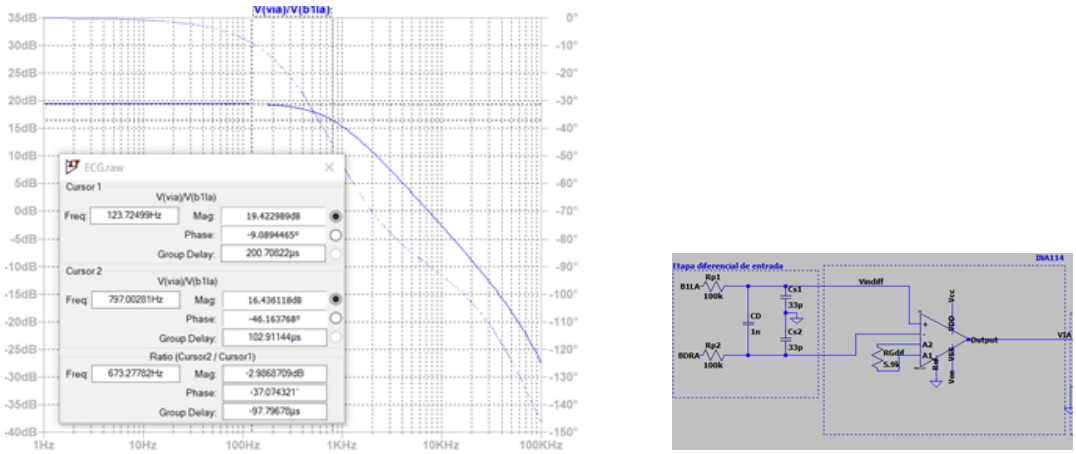

(a) Graph. (b) Schematics.

Figure 2.31: Bode diagram for the INA114 stage.

For the low-pass filter of first order stage the cut-off frequency is 1.44 kHz and the gain 37.9 (V/V), see in Figure 2.32a.

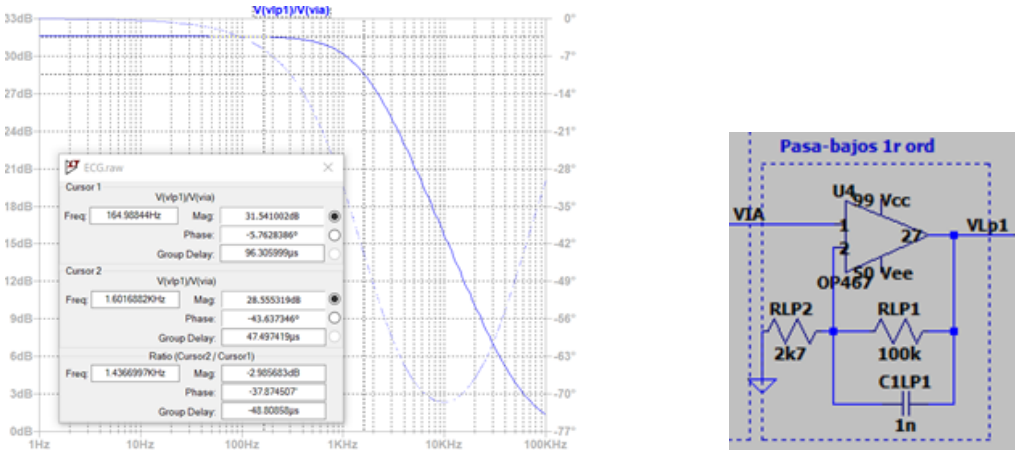

(a) Graph. (b) Schematics.

Figure 2.32: Bode diagram for the low-pass filter of first order stage.

For the Sallen-Key filter stage the cut-off frequency is 29.59 Hz and the gain 2.78 (V/V), see in Figure 2.33a.

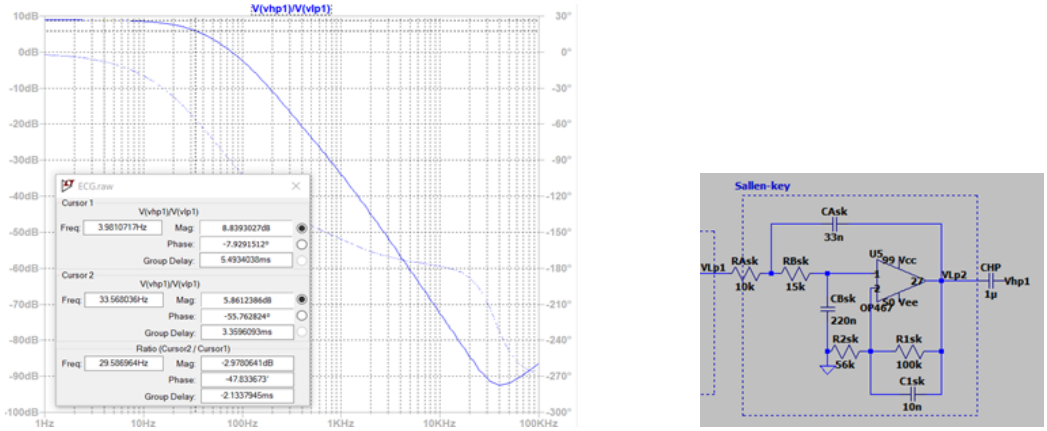

(a) Graph. (b) Schematics.

Figure 2.33: Bode diagram for the SK filter stage.

The Bode diagram of the whole system for the gain of 1000 (V/V) can be seen in Figure 2.34.

The Bode diagram of the whole system for the gain of 100 (V/V) can be seen in Figure 2.35.

The CMRR of the whole system for both gains can be seen in Figure 2.36.

Finally, a transient simulation with a sinusoidal signal of 2mVP and frequency of 10 Hz has ascertained the correct functioning (see in Figure 2.37.

The signals seen up until now have been the voltage obtained prior to the isolation side, which is not feasible to represent in LTSpice. Since the theoretical simulations are correct, the experimental part has been conducted.

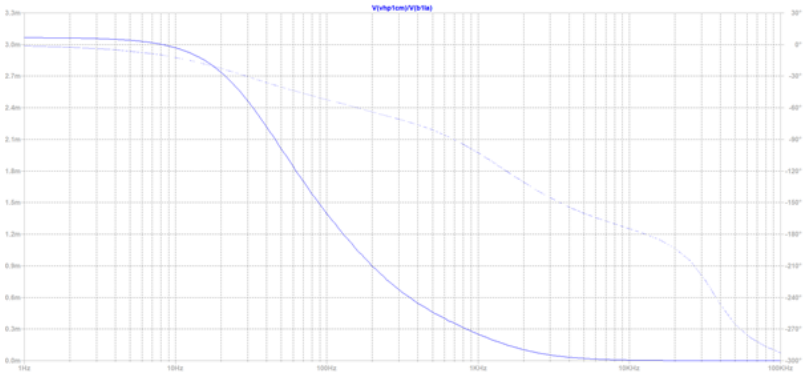

(a) Common mode configuration.

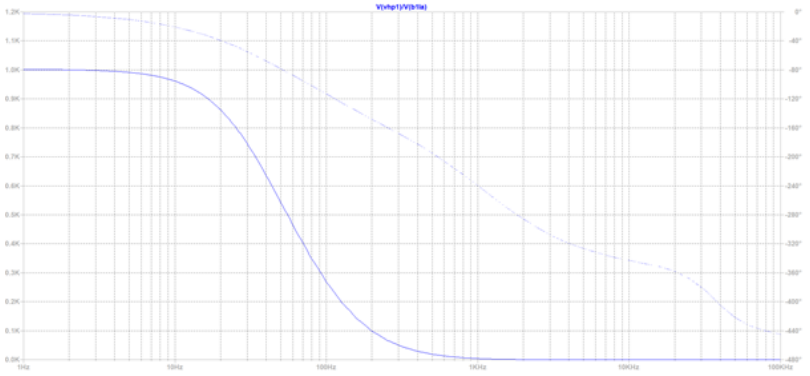

(b) Differential mode configuration.

Figure 2.34: Bode diagrams for the whole system with A = 1000.

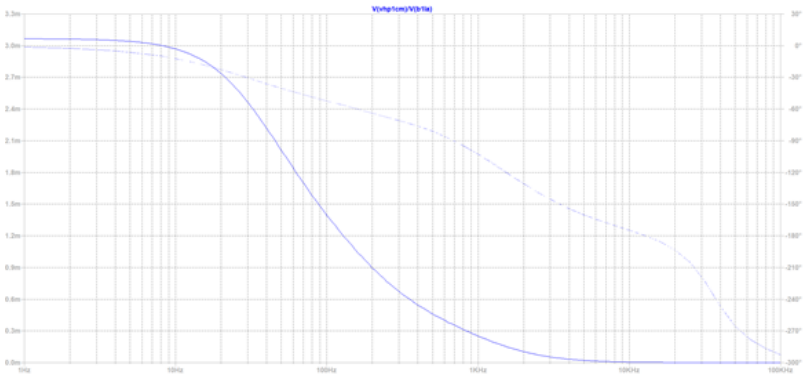

(a) Common mode configuration.

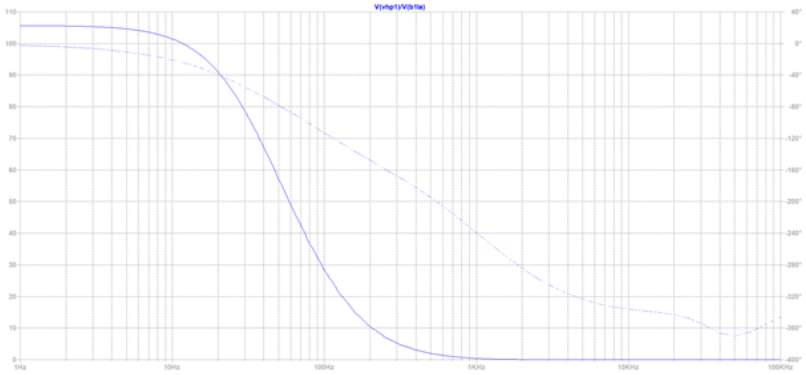

(b) Differential mode configuration.

Figure 2.35: Bode diagrams for the whole system with A = 100.

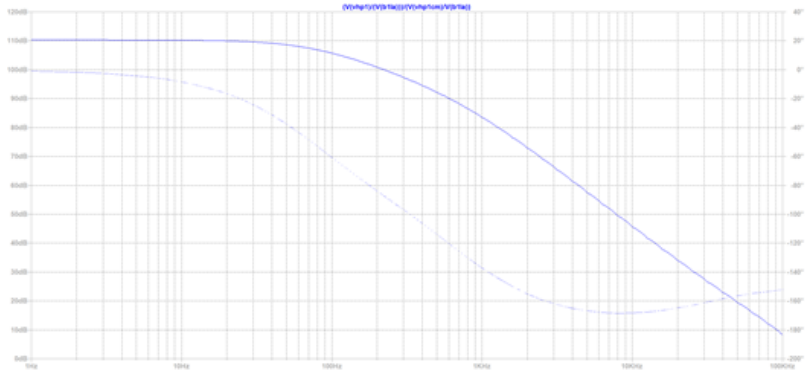

(a) A = 1000 (V/V). CMRR = 110 dB.

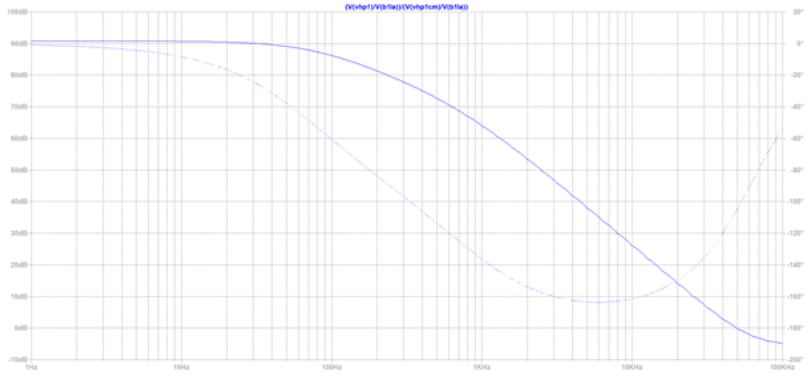

(b) A = 100 (V/V). CMRR = 90 dB.

Figure 2.36: CMRR representation.

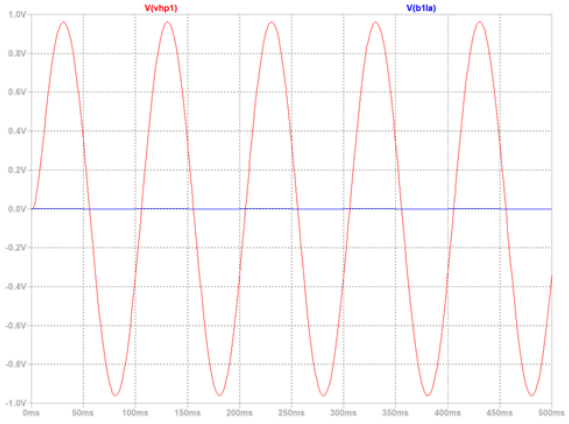

(a) A = 1000 (V/V).

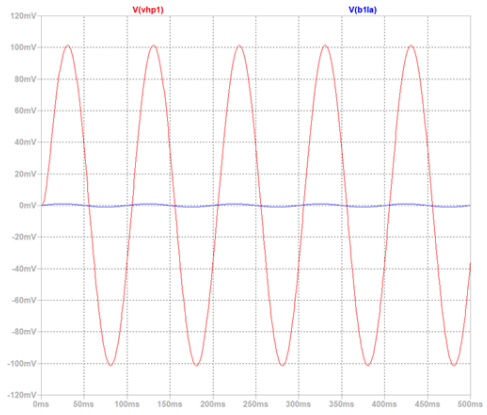

(b) A = 100 (V/V).

Figure 2.37: Transient simulation.

2.3 Results

With the design complete and described in the section above, the results are going to be analyzed and the key characteristics of the design examined. This section will highlight the performance specifications.

2.3.1 Protection Stage and High Frequency Filter

The assembly of this first stage of the project is depicted in the following figures:

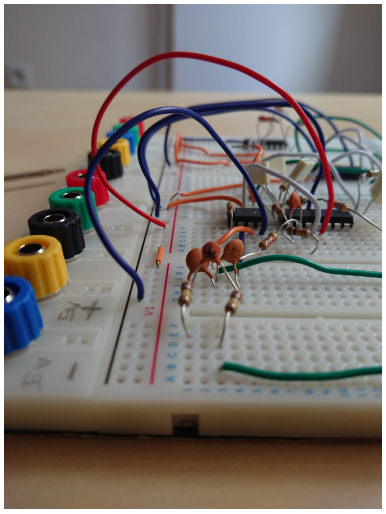

Figure 2.38: Protection stage and high frequency filter assembly

The experimental bodes for the differential and common mode configurations were:

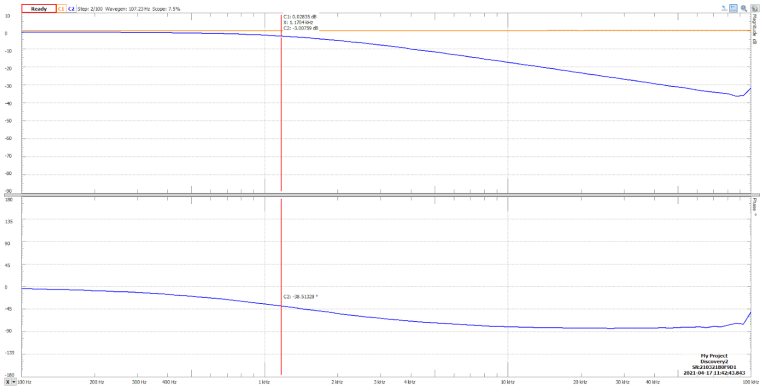

Figure 2.39: Differential mode BODE for the high frequency filter.

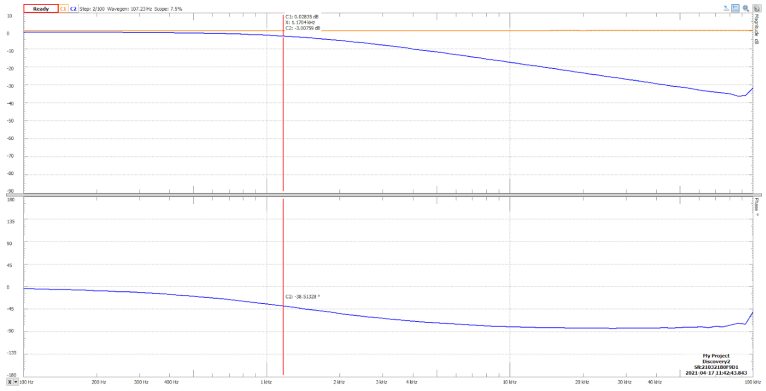

Figure 2.40: Common mode BODE for the high frequency filter.

The experimental cut-off frequencies were $f_c = 1.17kHz$ for the differential mode confiugration and $21.31kHz$ for the common mode configuration.

2.3.2 Differential Amplification

LM324 Experimental performance

Due to the limitations of the Analog Discovery 2 with input voltages, the experimental testing was limited to explore the BODE and CMRR for both amplifiers at G = 100 $\frac{V}{V}$. The reason behind was that for the higher gain, the voltage input should have been less than 6.6 mV. The limitation was that the Analog Discovery only accepts input voltages higher than 10 mV. So it was impossible to asses the higher gain, G = 740 $\frac{V}{V}$, in this experimental testing.

Despite the voltage limitations, the LM324 CMRR was tested with a gain of G = 100 $\frac{V}{V}$. The BODE for the differential mode configuration was:

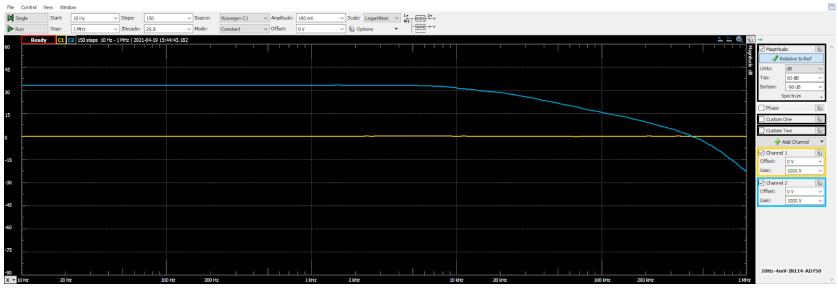

Figure 2.41: Differential mode of the LM325 for G = 100 $\frac{V}{V}$

In *Figure* 2.41 the DC gain was close to $40dB$, which was the value obtained in the LTSpice

simulations. And the cut-off frequency was around $13,34kHz$, also similar to the one in LTSpice. Next, the BODE for the common mode configuration was performed.

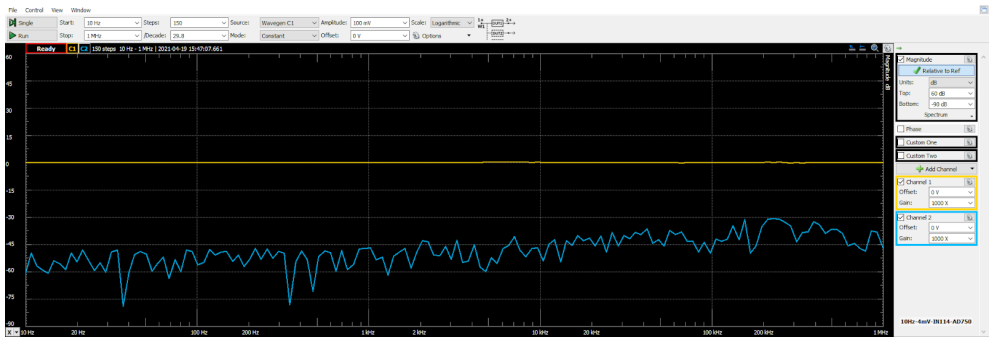

Figure 2.42: Common mode of the LM325 for G = 100 $\frac{V}{V}$

Unlike the differential gain in *Figure* 2.41, the common gain was unstable. Probably the instability was caused by noisy signals. Or maybe it was caused by the contact between the resistors and the capacitors wired at the protoboard. Although being an unstable common BODE, it can be seen in *Figure* 2.42 how the common mode signal is attenuated by its negative gain.
In addition, a transient simulation was performed with the same voltage characteristics as it was simulated in LTspice:

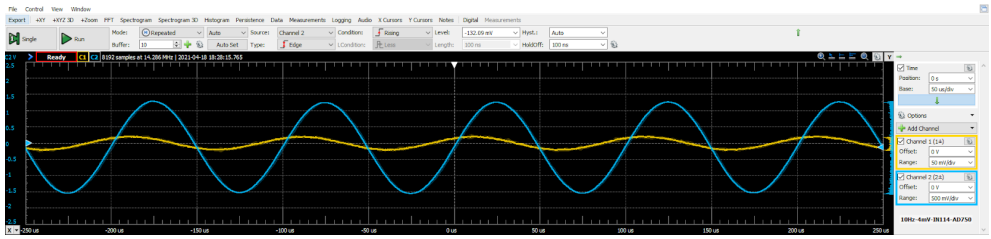

Figure 2.43: Transient simulation for the LM325 at G = 100 $\frac{V}{V}$

INA114 Experimental performance

The exact same experimental testing was performed over the INA114 amplifier. The resulted BODE and transient graphs were:

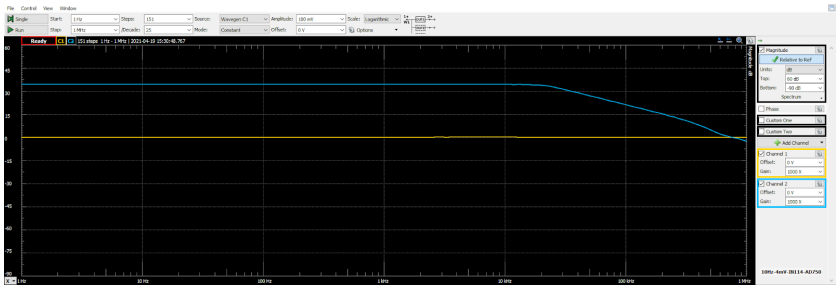

Figure 2.44: Differential mode of the INA114 for G = 100 $\frac{V}{V}$

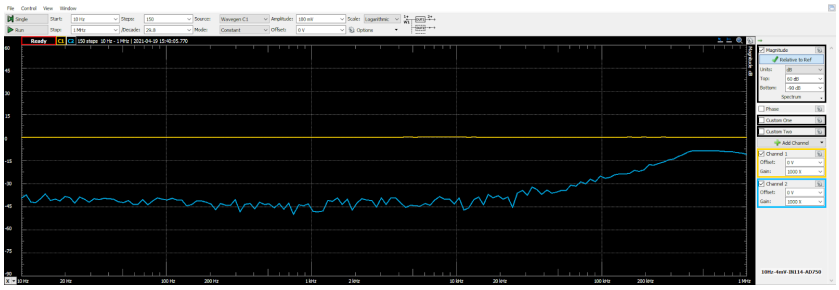

Figure 2.45: Common mode of the INA114 for G = 100 $\frac{V}{V}$

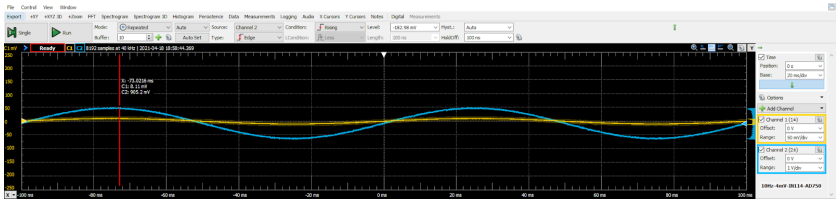

Figure 2.46: Transient simulation for the INA114 at G = 100 $\frac{V}{V}$

For the case of the INA114, the experimental cut-off frequency was $10.1Hz$, which was slightly different from the cut-off frequency found in the LTspice simulations. In addition, the common mode gain was more stable compared to the one for LM324. It is important for a common mode gain to be as much stable as possible. So it was important to consider this stability for the further decision among both amplifiers.
Finally, the CMRR of both amplifiers was compared using the data collected after the experimental measurements. As it can be seen in *Figure* 2.47, the INA114 presented a lower CMRR but more stable than the CMRR for the LM326. This stability was the main reason why the INA114 was finally selected to perform as the Instrumentation amplifier.

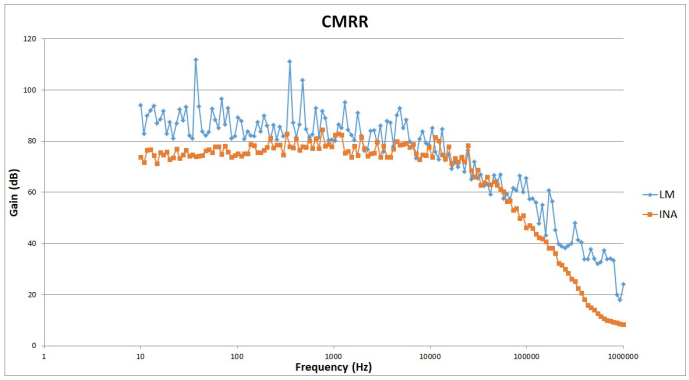

Figure 2.47: Experimental CMRR of the LM324 and INA114

2.3.3 Post Amplification Stage and Filter

The assembly of the first order filter and sallen-key is depicted in the following *Figure* 2.48:

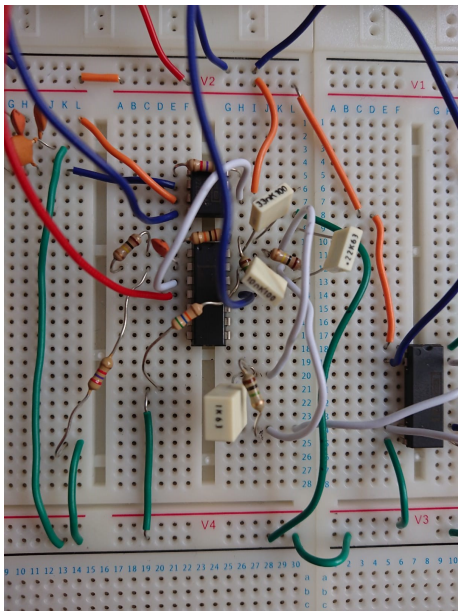

Figure 2.48: Assembly of the third stage: Post amplification and filtering

First order active filter testing

The corresponding BODE diagram for the first active filter is shown in the next *Figure* 2.49. As it could be seen in the graph, the cut-off frequency was 1.393 kHz, and the @DC gain

was 31,76 dB.

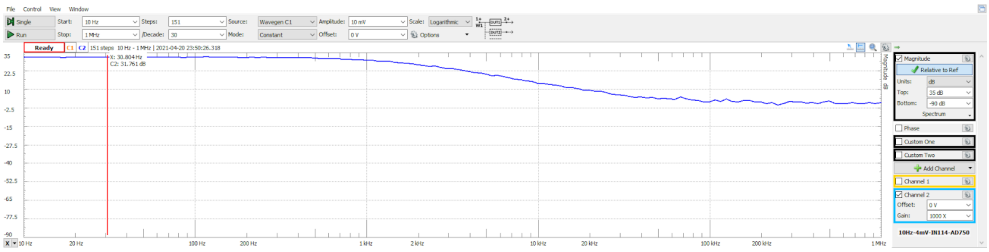

Figure 2.49: Experimental BODE for the first order active filter

Also a transient analysis with the same input signal as in the LTSpice simulations was performed. This time just to check how accurate was the amplifying performance of the active filter:

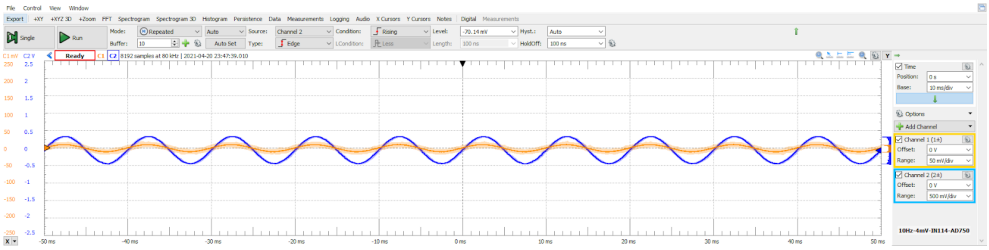

Figure 2.50: Experimental BODE for the first order active filter

Sallen-key testing

The corresponding BODE diagram for the Sallen-Key filter is shown in the next *Figure* 2.49. As it could be seen in the graph, the cut-off frequency was 17,229 kHz, and the @DC gain was 3.74 dB.

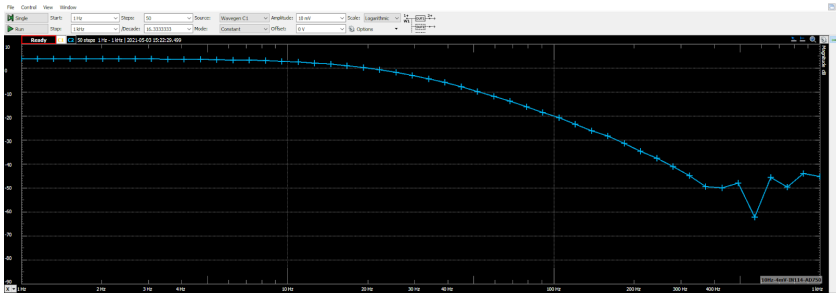

Figure 2.51: Experimental BODE for the Sallen-Key filter

2.3.4 Isolation, Acquisition and Representation of the Signal

The proper behaviour of the ISO122 has been checked experimentally using an input voltage of 5 V provided by a PCB called *ISOPow* that provides this isolated voltage using a battery of 12 V and a converter TracoPower TRV 1-1221M. To limit the voltage it has been build a voltage divider with two resistance of 100 kΩ. With this divider 2.5 V is the input voltage. The assembly can be seen in Figure 2.52.

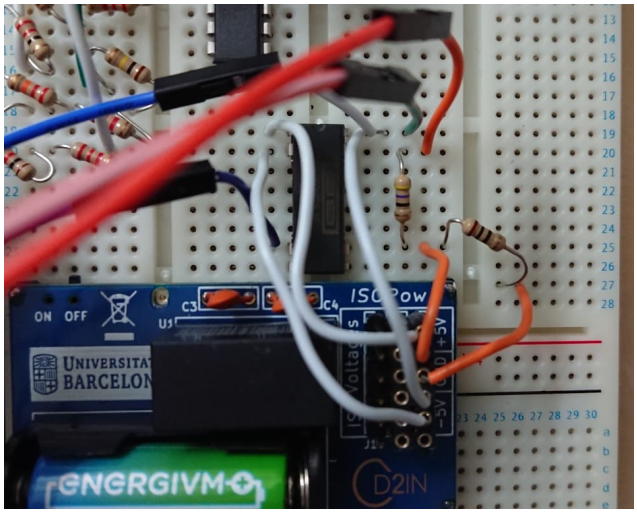

Figure 2.52: Assembly of the ISO122 and the *ISOPow*.

In Figure 2.53, it can be read the Channel 2 of the voltameter from the Analog Discovery that was connected to the output of the ISO122.

Figure 2.53: Voltameter at the output of the ISO122 (Channel 2).

Finally, the NI MyDaq has been used together with LabView to visualize the input and output voltages of the whole isolation stage. The ADC resolution of the NI myDAQ is 16 bits.

The Front Panel and the Block Diagram (see in Figure 2.54) enable the visualization of the signal (see in Figure 2.55).

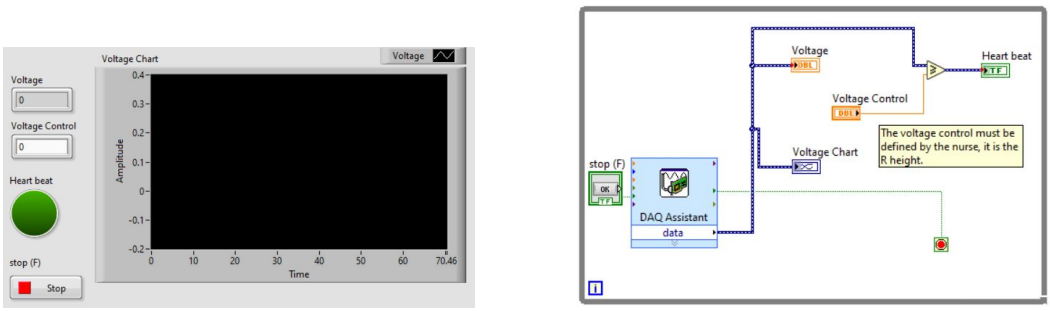

(a) Front Panel. (b) Block Diagram.

Figure 2.54: LabView application for the acquisition.

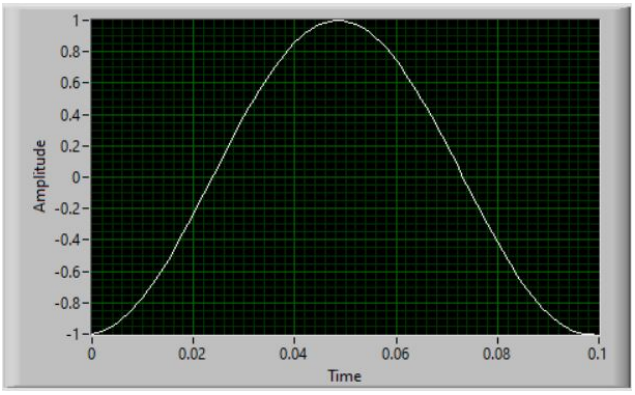

Figure 2.55: Visualization of the output signal for total gain of 1000 V/V.

The assembly of the ISO122 and the low pass filter based on the OP467 can be seen in Figure 2.56.

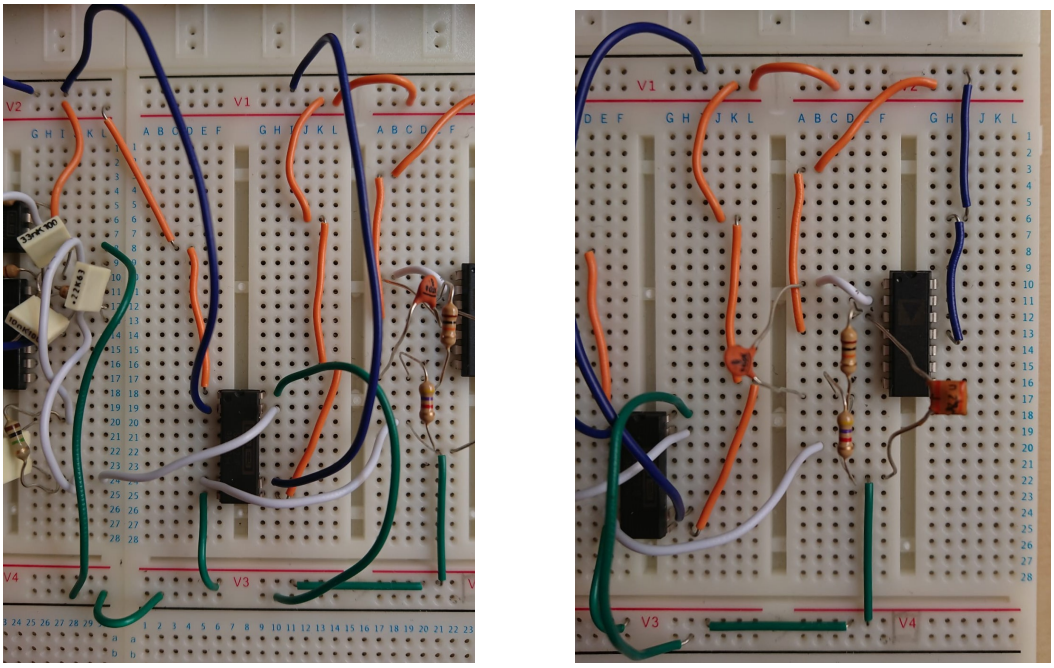

(a) ISO122. (b) OP467.

Figure 2.56: Isolation stage assembly on the *protoboard*.

2.3.5 Verification of the Design

The final configuration can be seen in Figure 2.57. It has been tested experimentally using a gain of 1000 (V/V) with a sinusoidal signal and with a patient (one of the students).
The output signal of the circuit, read with the Analog Discovery (acquisition system), is represented in Figure 2.58.

Finally, the circuit has been tested connecting three electrodes. One electrodes is connected on the right arm, another on the left arm (connected to the differential input), and the third one on the right leg (connected to ground). The last electrode is the reference electrode. The assembly can be seen in Figure 2.59 and 2.60 and the ECG in Figure 2.61. Wave P, segment PR, QRS complex, segment ST and wave T can be clearly seen. It is therefore a viable ECG with relevant information of the patient's heart conductive system.

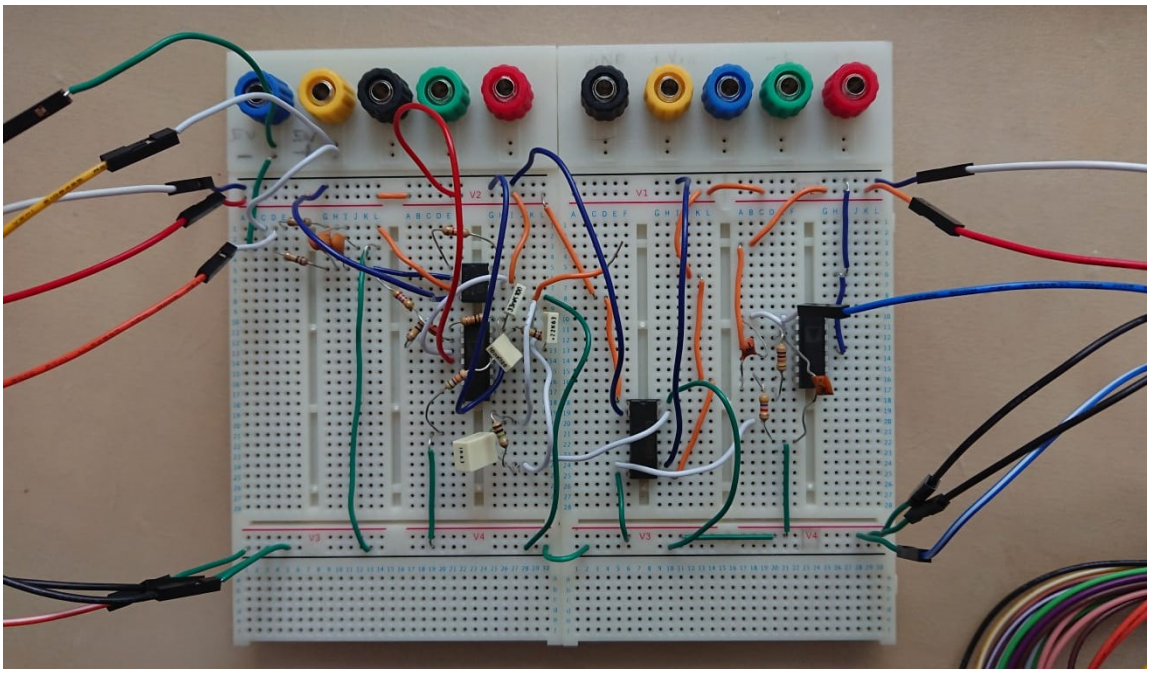

Figure 2.57: ECG circuit and connections to the two Analog devices.

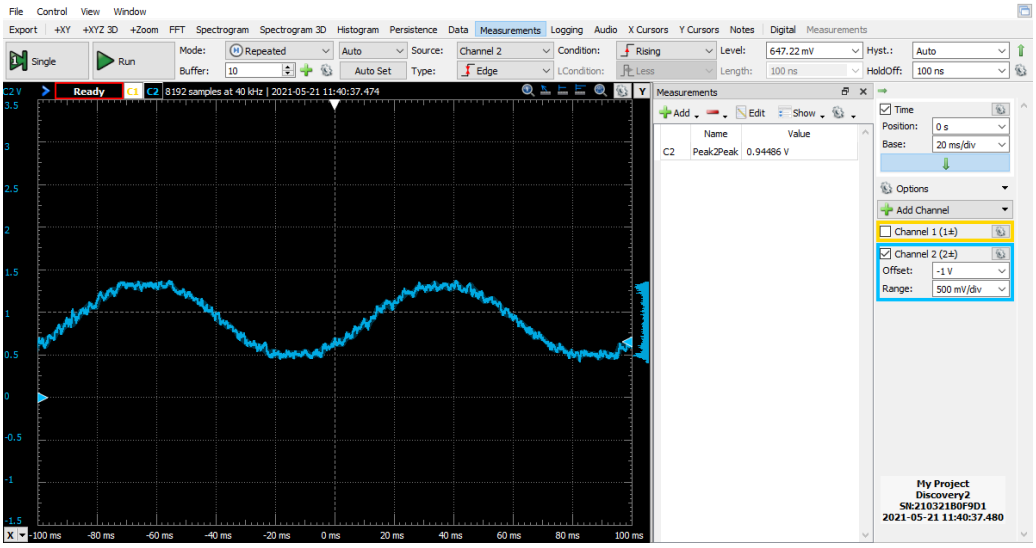

Figure 2.58: Output signal having introduced a sinusoidal signal of amplitude 2mVP and frequency 10 Hz.

Figure 2.59: Connecting the three electrodes to the patient.

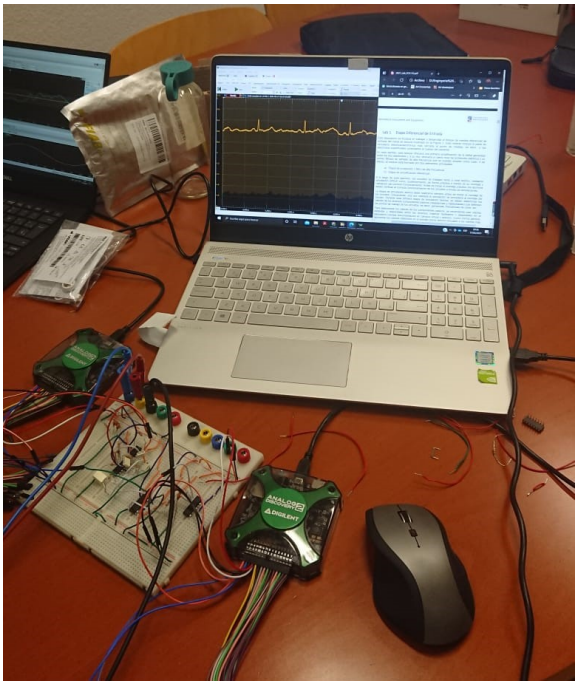

Figure 2.60: Setup of the testing session.

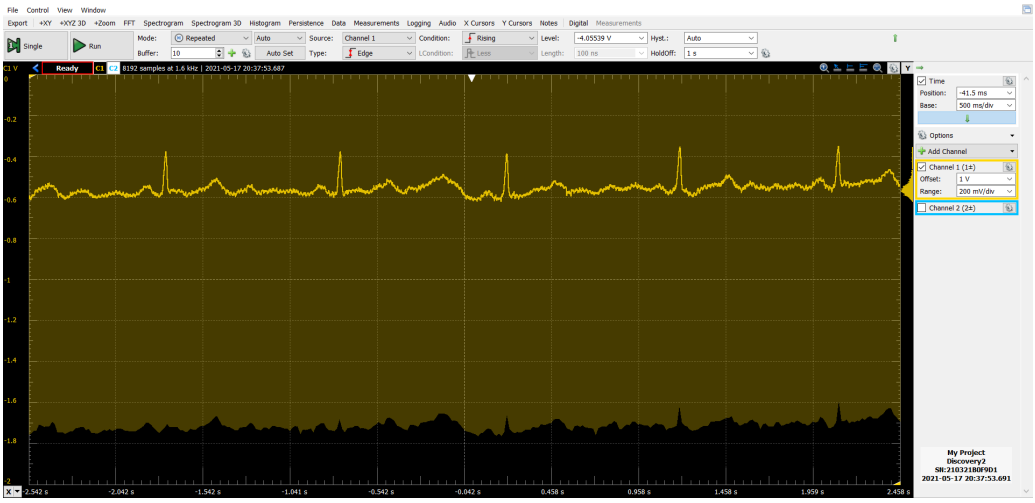

Figure 2.61: ECG recorded using three electrodes.

3 Execution Schedule

3.1 PERT

The start date was March 1, and the end was scheduled for May 17. The task definition is presented in table 3.1. The PERT can be read in figure 3.1. The critical path is remarked in red. In the next page, the GANTT chart can be read (figure 3.2).

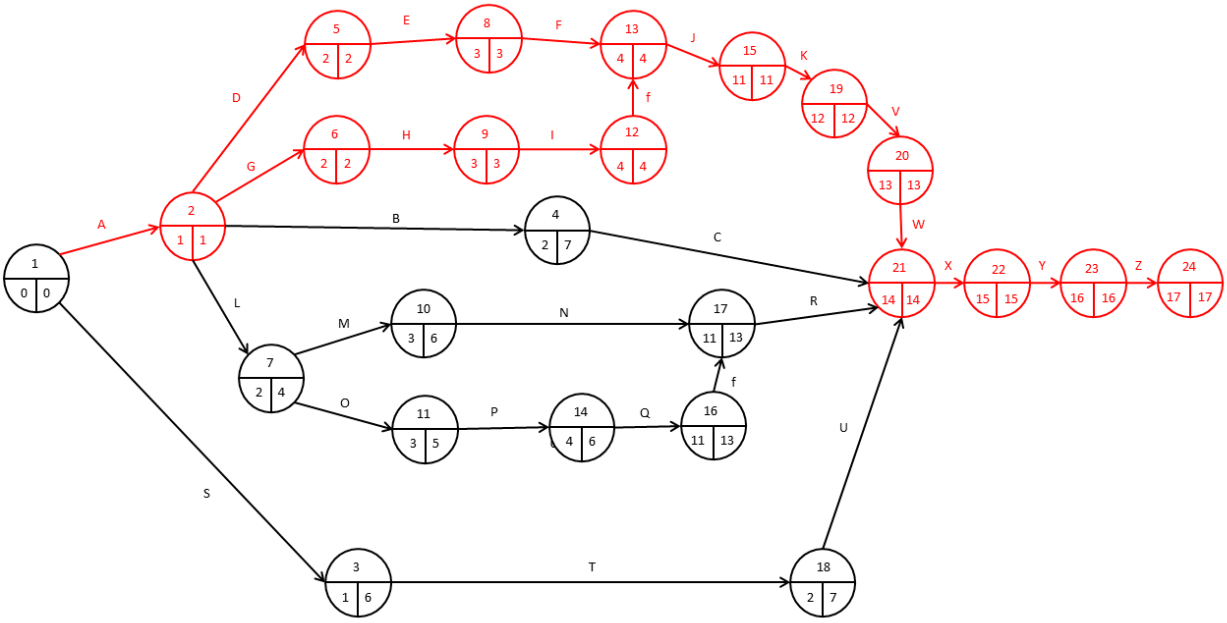

Figure 3.1: PERT Chart.

Task	Activity	Immediate predecessor	Duration (days)
RFI filter components selection	A	-	1
RFI Spice Simulation	B	A	1
RFI assembly and check	C	B	7
LM324 Rg selection	D	A	1
LM324 Spice Simulation	E	D	1
LM324 assembly and check	F	E	1
INA114 Rg selection	G	A	1
INA114 Spice Simulation	H	G	1
INA114 assembly and check	I	H	1
Comparisson study (AD, AC, CMRR) of both	J	F, I	7
Decision between LM324 and INA114	K	J	1
Post-amplification and filtering stage components selection 1st order low pass filter	L	A	1
1st order low pass filter Spice Simulation	M	L	1
1st order low pass filter assembly and check	N	M	7
Post-amplification and filtering stage components selection Sallen-key	O	L	1
Sallen-key Spice Simulation	P	O	1
Sallen-key assembly and check	Q	P	7
Joining both filters	R	N, Q	1
Study of ISO122 and assembly	S	-	1
ISO122 ouput filter Spice Simulation	T	S	1
Joining ISO122 and output filter and study	U	T	7
Component selection for a determined total gain	V	K	1
Spice Simulation of the whole circuit	W	V	1
Assembly of the whole circuit	X	C, R, W	1
Test with a sinusoidal signal	Y	X	1
Test with a volunteer	Z	Y	1

Table 3.1: Tasks' definition table.

3.2 GANTT chart

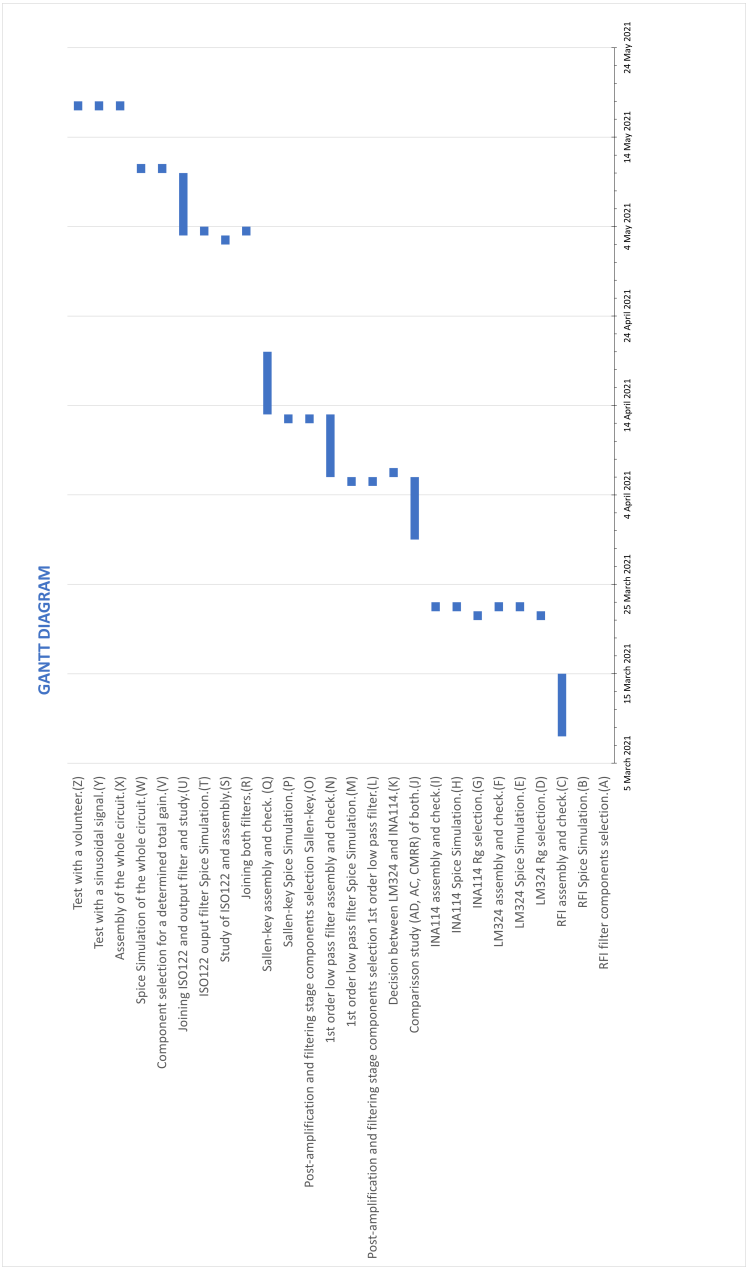

Figure 3.2: GANTT Chart.

4 Technical Viability

The SWOT analysis for the project can be seen in Table 4.1.

Strengths	**Weaknesses**
Guidance/supervision/support Teamwork Capability of working under pressure Good University installations Devices for teleworking Solid base of Spice	Limited diveristy of components Limited knowledge of assembling First time using some devices Environment noise Some material not available all the time
Opportunities	**Threats**
Cheap components High demand of medical portable devices	Medical regulations Solid competitors

Table 4.1: SWOT Analysis.

Conclusion

This memory described a complete ECG methodology and the development. The results have shown that this methodology was effective with small error compared with the theoretical simulations. The total error in the amplification circuit is approximately 10% . In the different tests, the signals that have been recorded present artifacts. Nevertheless, the captions of the patient testing probe that a real ECG signal can be recorded with enough quality to get information about patient health. The system work safely as an isolation amplifier was implemented.

This projects has achieved its objectives, but there are some points where it is possible to apply improvements.

Firstly, working with boards was a factor of noise. It would be better to use a printed circuit board (PCB) to integrate all together with less wires, improving this way the outcome.

Due to the lack of time, the LabView application for the acquisition has not been properly tested with the electrodes and the patient. Anyway, a possible improvement could be to convert the LabView project into a distributable application and improve the GUI with editable variables to write a report for each patient in a TDMS file.

Finally, the ECG signal is very susceptible to be affected by different kind of external and internal electric signals. The acquisition cables from the electrodes and the patient create a close circuit, if this close circuit is crossed by a magnetic field the outcome signal would be distorted. It must be convenient to use shielded-cables. Also, the resistances of the circuit can introduce thermal noise that can be reduce by cooling.

Bibliography

[1] Analog Discovery.
Quad Precision, High Speed Operational Amplifier.
URL: https://www.analog.com/en/design-center/design-tools-and-calculators/ltspice-simulator.html.
(accessed: 19.04.2021).

[2] Texas Instruments.
ISO122 Precision Lowest-Cost Isolation Amplifier.
URL: https://www.ti.com/.
(accessed: 05.05.2021).

[3] Texas Instruments.
LMx24, LMx24x, LMx24xx, LM2902, LM2902x, LM2902xx, LM2902xxx Quadruple Operational Amplifiers.
URL: https://www.ti.com/.
(accessed: 12.04.2021).

[4] On Semiconductor.
Operational Amplifiers, Single Supply, Quad.
URL: https://www.onsemi.com/.
(accessed: 12.04.2021).

[5] TBurr-Brown.
Precision INSTRUMENTATION AMPLIFIER.
URL: http://www.datasheetcatalog.com/datasheets_pdf/B/R/O/C/BROCHURE.html.
(accessed: 05.04.2021).

UNIVERSITAT DE BARCELONA

A special thanks to Jordi Colomer. His willingness to share his time and his knowledge with us was truly integral to the success of this project.